Deep Resources Engineering 3 (2026) 100231

Contents lists available at ScienceDirect

Deep Resources Engineering

journal homepage: www.keaipublishing.com/en/journals/deepre/

Full length article

Improving deconvolution reliability in well test analysis with an automated objective function

Mina S. Khalaf *

Cairo University, Egypt

ARTICLE INFO

Keywords:
Pressure transient analysis
Deconvolution
Objective function optimization
Reservoir characterization
Measurements uncertainty

ABSTRACT

Deconvolution is a mathematical technique that eliminates the effects of production rate variations in pressure transient data, enabling the recovery of a smoother pressure signal extended across both drawdown and buildup periods. This approach has distinct advantages over conventional analysis methods, including enhanced radius of investigation, improved derivative quality, and simplified use of existing interpretation techniques. Since the introduction of von Schroeter deconvolution method, as the first stable algorithm, in the early 2000s, several researchers have advanced the methodology by refining algorithms and improving the objective functions that govern their performance. Despite these developments, the definition of a robust and reliable objective function remains a challenge in achieving accurate deconvolution results. This study introduces a new objective function (NOF) for well test deconvolution that simplifies weighting schemes, eliminates subjective parameter tuning, and improves robustness under noisy conditions. Unlike earlier methods, the NOF assigns automated weights to pressure and rate measurements based on gauge accuracy, ensuring objective normalization of errors and removing the need for the unresolved flow rate regularization parameter. This streamlined approach not only reduces complexity but also enhances accuracy. The proposed noise-oriented NOF consistently outperformed traditional formulations across all simulated and field cases. In four synthetic examples with varying reservoir conditions and noise levels, the NOF successfully recovered smooth pressure responses and accurate flow rates, while the original von Schroeter and Levitan objective functions produced distorted or shifted signals and failed to adjust rates. Quantitative comparisons showed that this study produces a marked reduction in average deconvolution errors. This study enhances the stability and accuracy of deconvolution and offers a practical and superior tool for reservoir characterization, making it easier for engineers to extract meaningful reservoir properties, extend the radius of investigation, and reduce interpretation errors in real field applications.

1. Introduction

Deconvolution is a data processing technique employed in pressure transient analysis to extract a pressure response corresponding to a constant production rate from multi-rate well test measurements (Fig. 1). By removing the influence of rate variations in the recorded pressure signal, it generates a continuous drawdown pressure profile that spans both the flowing and shut-in phases of a test. Using the same data as conventional methods, deconvolution increases radius of investigation and captures boundary effects. Rather than replacing traditional analysis tools such as type curves or straight-line methods, deconvolution augments them by improving the quality and interpretability of the input data [1,2].

The process of deconvolution involves solving the convolution integral, also referred to as the superposition principle or Duhamel's principle, to determine the reservoir response function, denoted as $g(t)$. This integral expresses the pressure change $\Delta p(t)$ as a function of the production rate history $q(\tau)$ and the reservoir response to a unit impulse [3]. Mathematically, it is written as:

$$\Delta p(t) = p_0 - p(t) = \int_0^t q(\tau)\ g(t-\tau)\mathrm{d}\tau \tag{1}$$

$$g(t) = \frac{\mathrm{d}G}{\mathrm{d}t} \tag{2}$$

where, Δp is pressure drop, psi; p_0 is initial reservoir pressure, psi; p is measured pressure data, psi; q is measured flow rates, STB/D; G is constant-rate pressure drop, psi; and g is the derivative of the constant-

* Corresponding author.
E-mail address: minaskhalaf@gmail.com.

https://doi.org/10.1016/j.deepre.2025.100231
Received 31 August 2025; Received in revised form 9 November 2025; Accepted 12 November 2025
Available online 13 November 2025

rate pressure drop (G) with respect to time (t). g is also known as reservoir response function.

Interpolating rate and pressure response yields a solvable system for the equivalent drawdown profile. However, this inverse problem is inherently ill-posed, meaning that small measurement errors in pressure or rate can produce disproportionately large distortions in the computed response. Such data noise is common in practical well testing. Although early efforts to stabilize the deconvolution process date back to the late 1950s [4], robust algorithms only began to appear in the literature during the early 2000s [5–9]. To ensure numerical stability, modern deconvolution algorithms incorporate search-space constraints that guide the solution toward physically meaningful results despite data uncertainty. These stabilized techniques have been the subject of extensive study and refinement by numerous researchers [1,10–17].

Deconvolution offers several distinct advantages compared to traditional pressure transient interpretation methods. First, it yields a smoother pressure derivative curve than that obtained through numerical differentiation, which is often highly sensitive to measurement noise. Second, by reconstructing a pressure signal equivalent to a constant-rate drawdown across the full test duration, it enhances the effective radius of investigation, enabling better reservoir characterization. Third, deconvolution eliminates the need for superposition calculations, which are commonly used in conventional methods to correct for variable rate effects preceding the interpretation interval. However, the traditional analysis methods rely on numerical differentiation and superposition principles that produce a scattered and time-limited pressure derivative that deviates from the true solution.

Deconvolution serves additional purposes in pressure transient analysis. One such application is the mitigation of wellbore storage effects, which can obscure early-time pressure behavior [2,18–20]. Deconvolution techniques have also been successfully applied to more complex well test scenarios, including layered reservoir systems [21], multi-well configurations [22–24], and thermal response tests [25]. The application of deconvolution to improve pressure quality in tight carbonate formation is demonstrated by [26]. Ensemble-based algorithms have been introduced to quantify uncertainty and improve stability in pressure-rate deconvolution, providing a robust framework for both synthetic and field data [27]. Bayesian and hybrid formulations further integrate uncertainty quantification and physical constraints to achieve more reliable inversion under field noise [28]. In addition, machine learning has been increasingly adopted to automate model recognition and feature extraction in pressure transient analysis. Deep learning architectures, such as CNN and LSTM networks, have shown the ability to identify flow regimes and estimate reservoir parameters directly from raw pressure data [29,30]. Automated transient detection methods have also been proposed to identify valid pressure events in continuous production data, improving workflow efficiency and reliability in PTA and deconvolution [31]. A review of deconvolution applications in pressure transient analysis is presented by [32].

The main component in these deconvolution algorithms is the objective function, which quantifies the discrepancy between measured and modeled data and is minimized during the deconvolution process. Improving this function has been a focus of ongoing research. This study introduces a novel objective function designed to enhance deconvolution accuracy by incorporating measurement uncertainty and assigning automated, measurement-based weights to pressure and rate inputs. This formulation is compatible with existing stable deconvolution frameworks.

Despite major advances in stable deconvolution, current objective functions still rely on subjective or poorly constrained weighting which can bias solutions under realistic noise. This work addresses that gap by introducing a measurement-driven objective function (NOF) that (1) assigns automated, pointwise weights to pressure and rate data directly from gauge accuracy, objectively normalizing residuals, and (2) removes the need for a separate rate regularization parameter. Across simulated and field cases, NOF improves stability and fidelity of the recovered pressure signal and rates under noisy conditions, providing a practical path to more reliable deconvolution in routine well testing.

2. Stable deconvolution techniques

The introduction of a stable deconvolution algorithm is commonly attributed to [5]. Although the method represented a significant advancement, it exhibited limitations when applied to noisy data, particularly in flow rate measurements. Subsequent efforts by [6] and [33] addressed this issue by modifying the objective function to incorporate confidence measures for individual pressure and rate data points, thereby enhancing flexibility and robustness. This section presents a brief description of von Schroeter algorithm, and shows the improvements introduced to the objective function to enhance the deconvolution results.

In typical well testing practice, flow rates are recorded at the surface

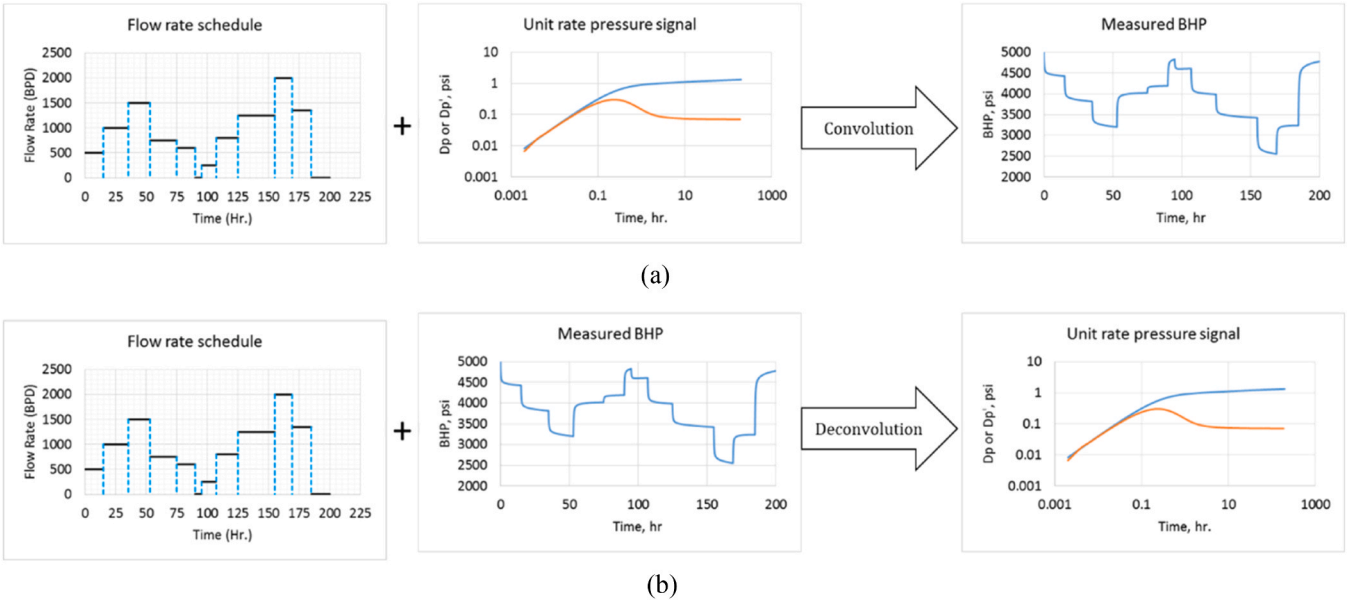

Fig. 1. Convolution (a) and deconvolution (b) schematic, showing how multi-rate pressure is transformed into an equivalent constant-rate response.

while pressure measurements are obtained downhole. The extent of noise present in these data can vary widely, influenced by the measurement equipment, wellbore conditions, and fluid properties. Previous studies report that pressure data noise typically ranges from 0.01 % to 1 %, while flow rate measurements may exhibit noise levels between 5 % and 15 % [33–36]. Despite advancements in surface flow rate measurement accuracy, test setups often rely on choke-regulated or tank-based methods, which introduce additional uncertainty.

Surface-based flow rate measurements present several inherent limitations. First, the rate recorded at the surface often differs from the rate actually experienced at the downhole pressure gauge. Second, the presence of a substantial wellbore volume between the gauge and the surface introduces lag and attenuation effects. Third, there is typically a time misalignment between pressure and rate data acquisition. These factors complicate the correlation between rate and pressure signals and diminish the reliability of downhole pressure interpretation. As a result, the effectiveness of using accurate pressure data in conjunction with surface-measured rates becomes restricted [37].

2.1. von Schroeter deconvolution technique

von Schroeter et al. [5] used a linear interpolation scheme for the pressure derivative between selected time nodes, and a stepwise interpolation scheme (Fig. 2) for the rates in the convolution integral (Eq. (1)). The resultant error measure accounts for errors in both rate and pressure measurements. The resulting objective function is treated as a total least squares problem (Appendix A).

To ensure the positivity of the resulting deconvolved pressure response, the authors used implicit constraints rather than explicit ones by encoding the algorithm in terms of the logarithm of pressure derivative function (Eq. (3)). On one hand, this encoding has the advantage of eliminating the external constraints. On the other hand, it introduces nonlinearity to the problem. An additional constraint term is used for the smoothness of pressure derivative as a measure of the total curvature of pressure derivative using the finite second derivative. von Schroeter et al. assumed that a unit slope line exists before the first time calculation node (this means that the pressure data, at least before the first time node, is dominated by WBS effects). The well test pressure derivative ($tg(t)$) is encoded according to the following equations:

$$z(\sigma) = \ln(t\ g(t)\,) \tag{3}$$

where $\sigma = \ln(t)$. z is logarithmic value of the well test pressure derivative. And σ is logarithmic value of time. Substituting Eq. (3) in the convolution integral (Eq. (1)) gives the model for pressures:

$$\Delta p_{\text{model}}(t) = \int_{-\infty}^{\ln(t)} \mathrm{e}^{z(\sigma)}\ q(t-\mathrm{e}^{\sigma})\ \mathrm{d}\sigma \tag{4}$$

The final formulation of the objective function is known as a nonlinear (separable) total least squares optimization problem. The standard method for solving this type of least squares problems is the variable projection algorithm [38,39]. The error function is defined as the sum of squares of errors/residuals of three terms: pressure match, rate match, and curvature penalty. The final form of the error function can be expressed as follows:

$$E(p_0, z, y) = \left\|p_0 Y_m - p - C(z)y\right\|_2^2 + \nu\left\|y - q\right\|_2^2 + \lambda\left\|Dz - K\right\|_2^2 \tag{5}$$

Here, the first term $\|p_0 Y_m - p - C(z)y\|^2$ quantifies the deviation between measured and modeled pressure data. The second term $\|y - q\|^2$ reflects the mismatch in flow rate estimates, weighted by the rate regularization parameter ν. The third term $\|Dz - K\|^2$ imposes a smoothness constraint on the pressure derivative through curvature penalization, with λ acting as the smoothing weight. Each component contributes to the overall stability and accuracy of the deconvolution solution. An initial estimate for the smoothing parameter λ is given by Eq. (6). The value of λ is suggested by von Schroeter et al. [5] until a smoothed derivative is achieved.

$$\lambda = \frac{\|\Delta p\|_2^2}{m} \tag{6}$$

where, Δp is pressure drop measurements, psi; and m is the number of pressure measurements. von Schroeter et al. specify one constant weighting value for each term in the objective function (Eq. (5)) to reflect its relative importance in the optimization process: unity for pressures, ν for rates and λ for smoothness. This objective function fails to provide a solution when the well test measurements suffer from high level of noise [40].

von Schroeter objective function includes two adjustable weighting parameters (ν and λ). von Schroeter et al. proposed expressions to evaluate these weighting parameters. These expressions do not always give the optimal values required for successful implementation of the technique. Eq. (6) gives an initial guess for λ; however, the final value is chosen subjectively. The authors stated that defining optimum values for these weighting parameters is an unresolved problem that requires future investigation.

2.2. Levitan deconvolution technique

Levitan [6] introduces two improvements to von Schroeter algorithm. First, Levitan's algorithm has the capability to process WBS-free well test data. Second, Levitan's objective function has the flexibility to assign different weights to well test observations to improve the deconvolution results (Appendix B).

von Schroeter algorithm was developed based on an assumption that the first time node is chosen in the WBS-dominated period. For solving the problem, Levitan rewrote the convolution integral (Eq. (4)) in a form

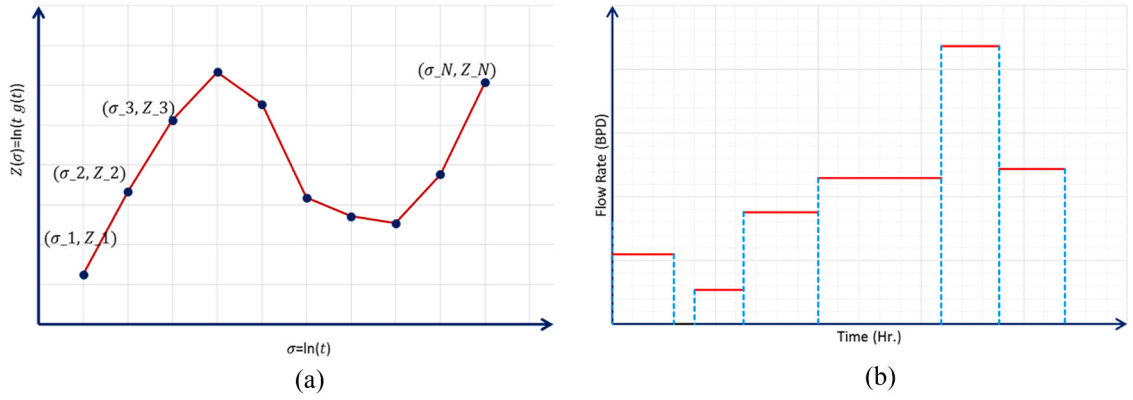

Fig. 2. Interpolation schemes for pressure derivative (a) and production rates (b): linear for pressure derivative and stepwise for rate.

that can handle the pressure drop at the first time node as a model parameter (unknown) to be found during the optimization process. To do this, Levitan extracted the first time node out of the integral such that the problem is optimized with no constraints on the data before the first node. If the first time node (σ_1) is selected to be small enough, the convolution integral (Eq. (4)) can be rewritten as follows:

$$\Delta p_{\text{model}}(t) = q(t)p_u(t_1) + \int_{\sigma_1}^{\ln(t)} q(t - e^{\sigma})\, e^{\sigma(\sigma)} d\sigma \tag{7}$$

where, $p_u(t_1)$ is the pressure drop at the first time node, psi; and $q(t)$ is flow rate as the time of pressure measurement. Expressing the convolution integral in this form made all the model parameters nonlinear and prevented handling the optimization problem as a separable least squares problem (that can be solved by the variable projection algorithm). Levitan used Dennis and Schnabel algorithm [41] for optimization. A drawback of this modification is that the optimization process can result in a negative value for the pressure drop at the first time node $p_u(t_1)$, as there are no constraints on the pressure drop at that time node. The final form of Levitan objective function is given by Eq. (8):

$$E(p_0,\ z,\ y,\ p_u(t_1)) = \frac{1}{2}\left\| \frac{p_0 Y_m - p - p_u(t_1)\ \widetilde{y} - \widetilde{C}(z)\ y}{\varsigma_p} \right\|_2^2 + \frac{1}{2}\left\| \frac{y - q}{\varsigma_q} \right\|_2^2 + \frac{1}{2}\left\| \frac{D\ z}{\varsigma_c} \right\|_2^2 \tag{8}$$

where, p_0 is initial reservoir pressure, psi; Y_m is constant vector of ones; p is the pressure measurements, psi; $p_u(t_1)$ is pressure drop at first time node, psi; $\widetilde{y}$ is flow rate at the time of pressure measurement, STB/D; and $\widetilde{C}(z)y$ is estimated from the integral term in Eq. (7). y and q are estimated and measured flow rates respectively, STB/D. D is a constant matrix and z is defined by Eq. (3). ς_p, ς_q, and ς_c are scaling parameters (error bounds) for pressure, rate, and curvature terms; respectively.

Levitan introduced the scaling parameters (ς_p, ς_q, ς_c) to normalize the individual terms of the objective function (pressure, rate, and curvature/smoothness terms). Each scaling parameter (also called error bounds) characterizes the uncertainty of the corresponding data point to be fitted. The values of the scaling parameters are set based on prior knowledge of the measured data quality. For all pressure measurements, Levitan set the scaling parameters (ς_p) to a constant value equal to the pressure gauge resolution (e.g. for quartz gauge, the resolution is 0.01 psi). For the flow rates, Levitan proposed the values of the error bound (ς_q) to be set based on the expected flow rate errors. For instance, high value of the scaling parameter is set for the cleanup period where the rate may not be measured. All scaling parameters of the curvature/smoothing term (ς_c) are set to the same constant value. Levitan found that 0.05 works well for the smoothing term. In other words, Levitan's objective function includes three scaling parameters (equivalent to weighting parameters in von Schroeter objective function). Two of these parameters have been given specific and clear values (gauge resolution for all pressure measurements and 0.05 for curvature term). For the rates term, Levitan suggested different values for the different rates (subjectively chosen based on the accuracy of rate measurements). However, Levitan did not present how large or small the chosen values will be.

2.3. Pimonov deconvolution technique

Pimonov et al. [33] introduces modifications to the deconvolution objective function to mitigate the effects of unreliable pressure and rate measurements on the deconvolution results. The authors implemented their objective function to von Schroeter and Levitan algorithms. In addition to the scaling parameters (error bounds) presented by Levitan, Pimonov's objective function uses variable weights for the individual measured well test data points. Pimonov et al. rewrote the objective functions of von Schroeter and Levitan as follows:

$$Error = \frac{1}{2}\sum_{i=1}^{N_p} {w_{p_i}}^2 \left[\frac{p_0 - p_i - \Delta p_{\text{model}}}{\sigma_p}\right]^2 + \frac{1}{2}\sum_{j=1}^{N_q} {w_{q_j}}^2 \left[\frac{q_j - q_j^u}{\sigma_q}\right]^2 + \frac{1}{2}\sum_{k=1}^{N-1} \left[\frac{k_k}{\sigma_c}\right]^2 \tag{9}$$

where, p_0 is initial pressure, psi; p_i is measured pressure, psi; and Δp_{model} is the pressure model (follows Eq. (4) for von Schroeter algorithm, and Eq. (7) for Levitan algorithm). q_j and q^u are measured and estimated flow rates (STB/D), respectively. k_k are curvature constraints. N_p, N_q, and N are number of measured pressures, measured rates, and time nodes; respectively. σ_p, σ_q, and σ_c are the error bounds (originally introduced by Levitan as ς_p, ς_q, and ς_c in Eq. (8)). w_{p_i} and w_{q_j} are new sets of variable weights introduced by Pimonov et al. for pressure and rate measurements, respectively.

Pimonov et al. set the values of each error bounds (σ_p, σ_q) to the standard deviation of the error in the measured well test data. They suggested values of 0.01 psi for pressures and 10 BPD for rates as initial values. Depending on the smoothness of the solution, Pimonov et al. changed the error bound by order of magnitude (multiplying or dividing by 10) and then for fine tuning by one third of the order of magnitude ($\sqrt[3]{10}$). For curvature constraints, Pimonov et al. found that σ_c= 0.05 (that was suggested by Levitan) works well.

The values w_{p_i}, and w_{q_j} represent the weights to the measured pressures and rates, respectively. Pimonov et al. suggested that the values of these parameters should range from zero to one depending on the quality of the observed/measured well test data. The weights are set to one for the most accurate measurements and zero for the least accurate measurements. The rest of the weights are distributed between zero and one. Pimonov et al. found that there was no need for using variable weights in the curvature term.

Pimonov's objective function [33] includes five weighting sets of parameters: two parameters for the pressure term (w_{p_i}, and σ_p), two parameters for the rate term (w_{q_j}, and σ_q), and one parameter for the curvature/smoothness term (σ_c). The authors set σ_c to a constant fixed value of 0.05 (the same as Levitan's). The values of σ_p and σ_q are set to initial values of 0.01 and 10, respectively. These values are then adjusted subjectively until a smooth pressure derivative curve is obtained. The authors suggested a range (from zero to one) for setting the parameters w_{p_i} and w_{q_j} (these represent one weight value for each pressure measurement and another weight value for each rate measurement going into the deconvolution calculations). However, they did not show a procedure to assign specific values between zero to one to individual points. In addition, the large number of weights to be specified by the user can be cumbersome without appropriate guidelines, which makes it difficult to exploit in practice as stated by [11].

3. Developed methodology

This study builds upon the foundational contributions of von Schroeter et al., Levitan, and Pimonov et al. [5,6,33], and seeks to address ongoing challenges in deconvolution under noisy well test conditions. The primary aim is to introduce a revised objective function that can be integrated with existing stable algorithms. This modified formulation is designed to enhance performance when dealing with measurement uncertainty and variability, offering improved reliability and accuracy in deconvolution outcomes across a wide range of well test scenarios.

A modified version of the deconvolution objective function was developed to improve solution robustness and reliability. This revised form offers two primary advantages: (1) it simplifies the complex weighting formulations proposed by earlier researchers [5,6,33], as the new objective function includes only one weighting parameter for each term (pressure, rate, and smoothness/curvature terms), (2) it enables the automatic determination of weights based on the known accuracy of

pressure and rate measurement instruments, and (3) it produces more accurate results of deconvolved pressure signal and flow rates than the previous techniques. The resulting objective function, which incorporates these improvements, is defined as follows:

$$Error = \sum_{i=1}^{Np} \left(w_{pi}\,[p_{mi} - p_{Mi}]\right)^2 + \sum_{j=1}^{Nq} \left(w_{qj}\left[q_{mj} - q_{Mj}\right]\right)^2 + \lambda ||D\,z - K||_2^2 \tag{10}$$

where, w_{pi} and w_{qj} are weights for pressure and rate measurements, respectively. p_{mi} and p_{Mi} are measured and estimated (calculated) pressures, respectively. The pressures (p_{Mi}) can be modelled by Eq. (4) for von Schroeter technique or Eq. (7) for Levitan technique. q_{mj} and q_{Mj} are measured and estimated (calculated) rates, respectively. N_p and N_q are numbers of pressure and rate measurements, respectively. The smoothing term is kept the same as given by von Schroeter et al. [5].

The weight values w_{pi} and w_{qi} are set such that the contributions of the individual well test measurements (pressures and rates) to the objective function are equalized/normalized. This can be accomplished by setting the pressure and rate weights according to the following expressions:

$$w_{pi} = \frac{1}{G_p{}^{*}p_{mi}} \tag{11}$$

$$w_{qj} = \frac{1}{Gq^{*}q_{mj}} \tag{12}$$

where, G_p and G_q are the expected errors of pressure and rate gauges, respectively. These values (gauge accuracy) are often provided by gauge manufacturers, hence, they are easily available to the well test analyst. The available technology can measure pressures with error levels of 1 % and below. Rate measurements are in error by 5 %–15 %, i.e. $G_p = 0.01$ and $G_q = 0.15$ [42,43]. For illustration, consider typical manufacturer specifications: a downhole pressure gauge with an accuracy of 0.3 % full-scale at 5000 psi, and a rate meter with 10 % accuracy at 200 STB/D. These values yield error bounds of 15 psi for pressure and 20 STB/D for rate. Substituting these accuracies into Eqs. (11) and (12) provides weighting factors of 0.0667 (for pressure) and 0.05 (for rate) used in the objective function, normalizing residuals by actual measurement precision.

Measurement accuracy for both pressure and rate is treated as a percentage of the reading, so that Eqs. (11) and (12) normalize residuals by the local measurement precision. If instrument accuracy varies with value, the manufacturer guidelines are used. Example: suppose a pressure sensor has 0.1 % of reading for $p \leq 3000$ psi and 0.2 % of reading above. Then for a 2,000-psi reading, $w_p = 1/\,(0.001 \times 2000) = 0.5\ \text{psi}^{-1}$. For a 5,000-psi reading, $w_p = 1/\,(0.002 \times 5000) = 0.1\ \text{psi}^{-1}$.

The specification of smoothing term weighting parameter (λ) follows the procedure given by [5]. The procedure entails employing Eq. (6) to give initial value. The final λ is refined by visual judgment of the pressure-derivative curve (smooth but not over-smoothed), preserving expected early-time behavior, and showing no spurious late-time trends.

The new objective function has two main advantages over the previous work. These advantages are:

1. The new objective function assigns a different weight for each pressure and rate point (Eqs. (11) and (12)). This allows the normalization of the error contributions from the different well test measurements in the optimization process. The weights are specified automatically and objectively based on the accuracy of gauges used in measurements.
2. It excludes the flow rate regularization parameter (presented in von Schroeter objective function). Obtaining a good value of this parameter (ν) is not easy. Therefore, the new objective function solves the problem of the selection criteria of this parameter, which was reported as unresolved problem by von Schroeter et al. [5].

Although this mechanism of setting weights to simulated data sets using two deconvolution algorithms (von Schroeter and Levitan) is applied, other stable algorithms can also benefit from the new objective function [7–9]. For von Schroeter and Levitan algorithms, the number of time nodes to evaluate the deconvolved response are set to thirty points. These nodes are uniformly distributed on logarithmic scale, as suggested by the authors. This number was found sufficient to represent the pressure and derivative profiles with the required level of detail. Adding more points would increase the number of unknowns in the solution, which could make the results less stable without a noticeable improvement in accuracy. The selected number provides a balance between numerical stability and the resolution needed to capture the pressure behavior. A computer program was developed to compute the deconvolved signal using both von Schroeter and Levitan algorithms for testing of different objective functions and validation of results.

A single rule is used across all cases for the selection of λ: (1) Initialize λ from Eq. (6) of von Schroeter as the starting value. (2) Compute the deconvolved pressure and its derivative; if the derivative shows over-smoothing (muted curvature near expected early-time behavior) decrease λ; if it shows noise-induced oscillations or spurious late-time trends, increase λ. (3) Iterate until the derivative is smooth but not over-smoothed and preserves expected early-/late-time behavior. The complete workflow of the NOF-based deconvolution method, including weight computation, λ refinement, and objective minimization, is summarized in Algorithm 1.

Table 1
Description of the simulated cases.

		Example 1	Example 2	Example 3	Example 4
h (ft)		30	80	60	75
k (md)		33.3	55	65	30
Skin		0	−3	−2	0
Porosity (%)		10	21	17	9
P_i (psi)		5000	4000	5500	3000
B_o (bbl/STB)		1.1	1.3	1.22	1.15
Viscosity (cp)		1	6	3	5
r_w (ft)		0.3	0.3	0.3	0.3
C_t (psi^{-1})		3×10^{-6}	5×10^{-6}	5×10^{-6}	5×10^{-6}
WBS (bbl/psi)		0.01	0.007	0.05	0.005
Boundaries		Infinite-acting	Infinite-acting	No-flow circular ($r_e = 1250\,ft$)	One fault ($L = 500\,ft$)
Reservoir		Homogeneous	Two porosity PSS	Homogeneous	Homogeneous
Omega		-	0.1	-	-
Lambda		-	8×10^{-7}	-	-
Noise level	Pressure (%)	0.5	0.25	0.1	1
	Rate (%)	33	40	50	18

Algorithm 1. (*NOF-based deconvolution workflow, showing inputs, outputs, and calculation steps.*)

Inputs: measured pressures p, measured rates q, gauge-accuracy specifications (G_p, G_q), and algorithm (von Schroeter, Levitan).

Outputs: deconvolved constant-rate pressure G(t), pressure derivative g(t), and reconstructed rates q.

Workflow steps:

1. Build objective function structure per Equation (10).
2. Compute measurement weights using Equations (11) and (12):
   2.1. For each pressure point i, set w_p,i from G_p.
   2.2. For each rate point j, set w_q,j from G_q.
3. Set smoothing weight λ: initialize from Equation (6); refine to obtain a smooth but not over-smoothed derivative per the stated criterion.
4. Select forward model per algorithm:
   4.1. von Schroeter: pressure model via Equation (4); separable least-squares with variable projection.
   4.2. Levitan: pressure model via Equation (7) with p_i as unknown; non-separable least-squares.
5. Optimize objective (using standard MATLAB functions):
   5.1. von Schroeter: variable-projection with "lsqnonlin", analytic Jacobian.
   5.2. Levitan: "lsqnonlin" ("Levenberg–Marquardt"), analytic Jacobian.
6. Check convergence; if derivative shows over-smoothing or oscillations, adjust λ and repeat Step 5.
7. Return G(t), g(t), and q; report (G_p, G_q), λ, and solver settings with results.

4. Simulated cases

This section presents the applications of the proposed objective function to four simulated cases. The testing data sets are generated for a variety of well/reservoir models and include different levels of noise. The properties used in generating the pressure transient data of the examples are given in Table 1. The skin values in these simulated cases were set to zero or negative to represent clean or stimulated wells. The total compressibility values (c_t) include both rock and fluid compressibility components and represent the overall behaviors for slightly compressible systems.

4.1. Simulated case 1

The case simulates a 30-hour test (two flow periods followed by a shut-in period) generated for a homogeneous reservoir with infinite reservoir boundary. The noise level added to the data is 0.5 % for pressures (1175 pressure points of errors normally distributed with a standard deviation of 11.3 psi) and 33 % for rates. The well test data is given in Figs. 3 and 4. In these figures, the exact data are illustrated in red and the erroneous/noisy data in blue. The new objective function (NOF) is implemented using von Schroeter and Levitan techniques. The results are given in Figs. 5–7, along with the results from the original objective functions (Eqs. (8) and (9)). The weighting parameters are listed in Table 2. In Figs. 5 and 7, the deconvolution results from the

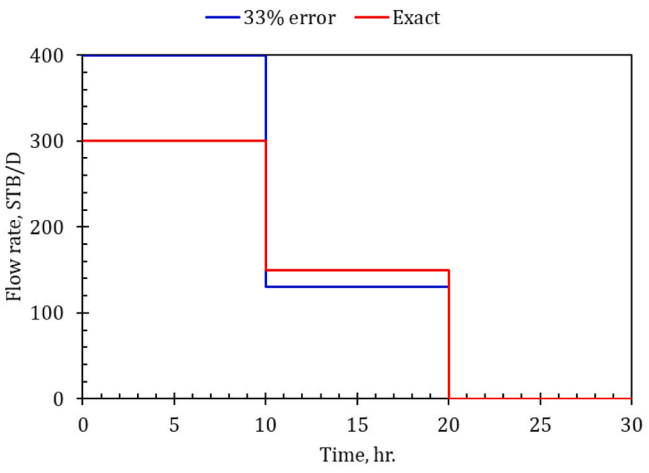

Fig. 3. Flow rate schedule – simulated example 1.

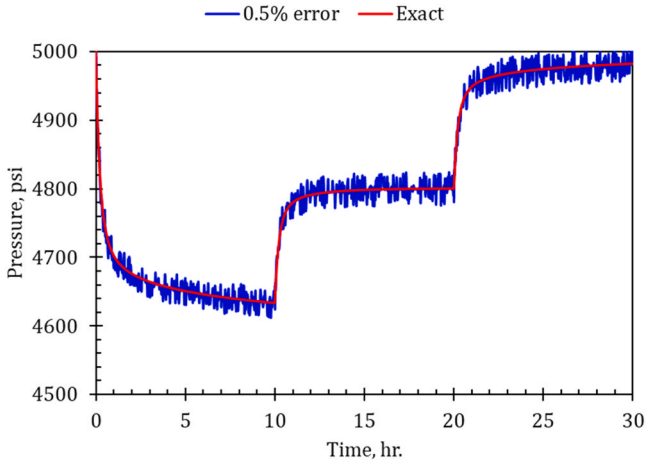

Fig. 4. Pressure profile – simulated example 1.

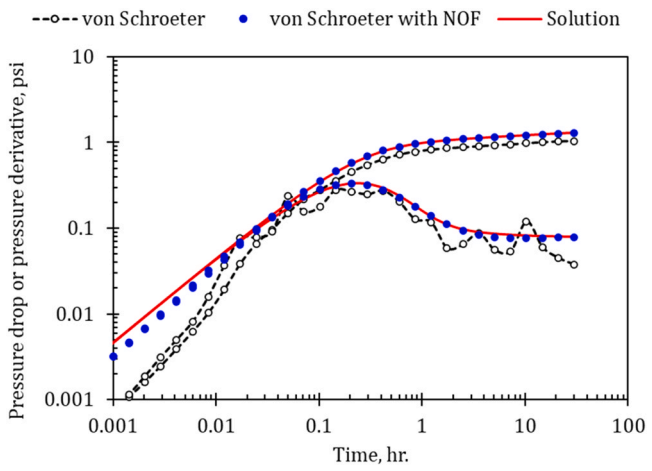

Fig. 5. Results from modified and original von Schroeter objective function - simulated example 1. The NOF yields smoother pressure and closer match to the true response.

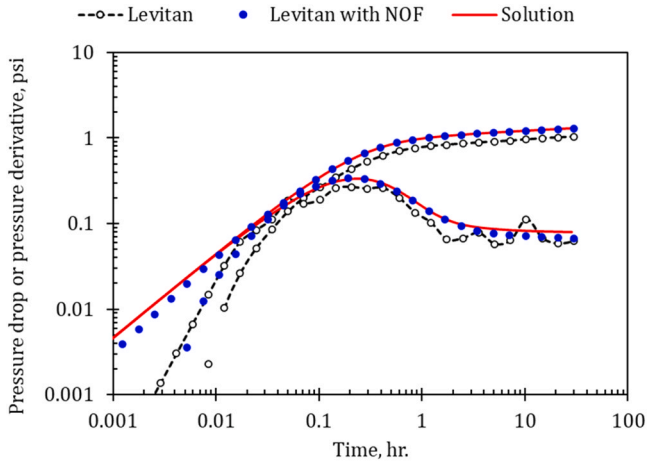

Fig. 6. Results from modified and original Levitan objective function – simulated example 1. The NOF tracks the true response except at earliest times.

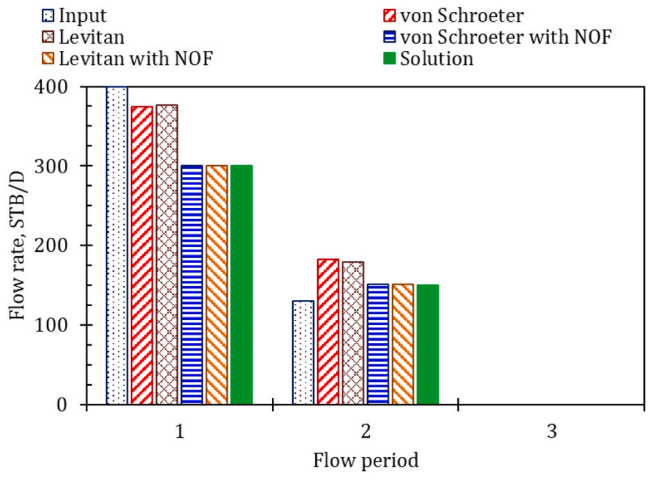

Fig. 7. Comparison of flow rates resulting from deconvolution with different techniques – simulated example 1. NOF recovers correct rates; originals fail to adjust toward the true schedule.

Table 2
Weighting parameters used with NOF and original objective functions.

	New Objective Function		Original Objective Function				
	von Schroeter	Levitan	von Schroeter	Levitan			
	λ	λ	ν	λ	ς_p	ς_q	ς_c
Example 1	1.0E3	1.0E3	0.71	1.0E3	0.01	10	3.2E−3
Example 2	3.2E3	5.6E3	0.54	3.2E3	0.01	10	1.8E−3
Example 3	3.2E3	5.6E3	0.67	3.2E3	0.01	10	1.8E−3
Example 4	7.5E2	5.6E2	0.52	1.0E2	0.01	10	7.0E−4

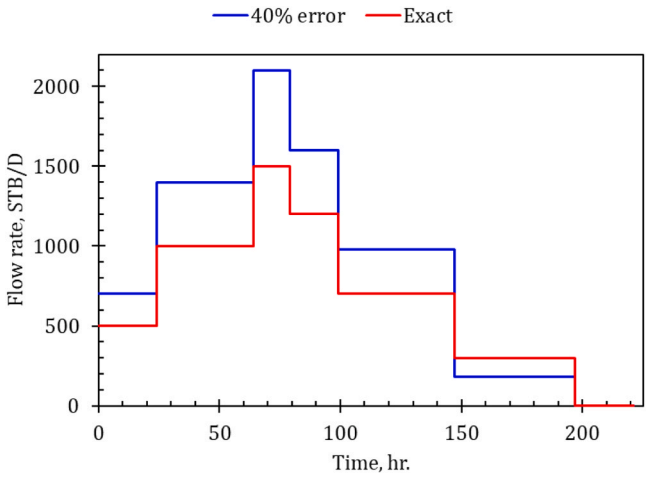

Fig. 8. Flow rate schedule – simulated example 2.

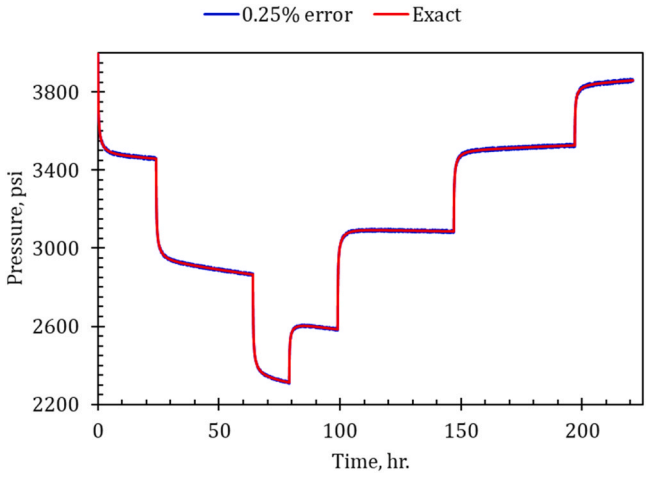

Fig. 9. Pressure profile – simulated example 2.

original von Schroeter and Levitan objective functions are presented in dashed line with circles. The results of the NOF are given as blue points, and the correct solution is shown as red line. The resultant pressure data from the new and original objective functions with von Schroeter algorithm are depicted in Fig. 5. The results from the new objective function are in good agreement with the true solution. Due to the noise in the data, the original von Schroeter algorithm generates oscillating pressure signal. The results from Levitan algorithm are presented in Fig. 6. The new objective function gives a pressure signal that matches the true solution very well, except for slight deviation in the beginning (before 0.01 hrs. in time). However, the original Levitan algorithm yields highly distorted response. The estimated flow rates are given in Fig. 7. The figure compares the resultant rates from von Schroeter and

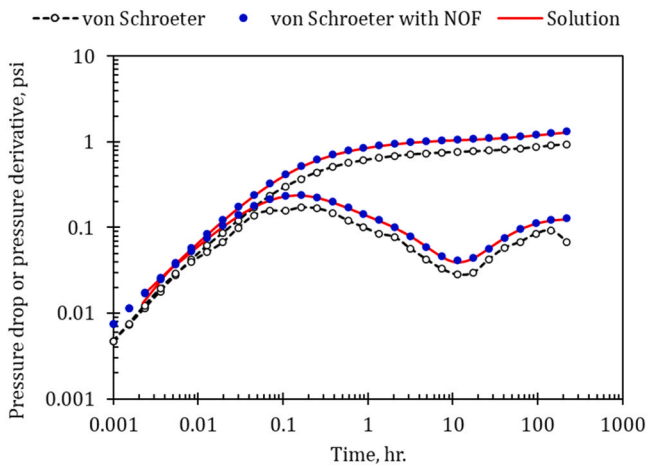

Fig. 10. Results from modified and original von Schroeter objective function – simulated example 2. Original is shifted and suggests false late-time trend; NOF aligns with the true response.

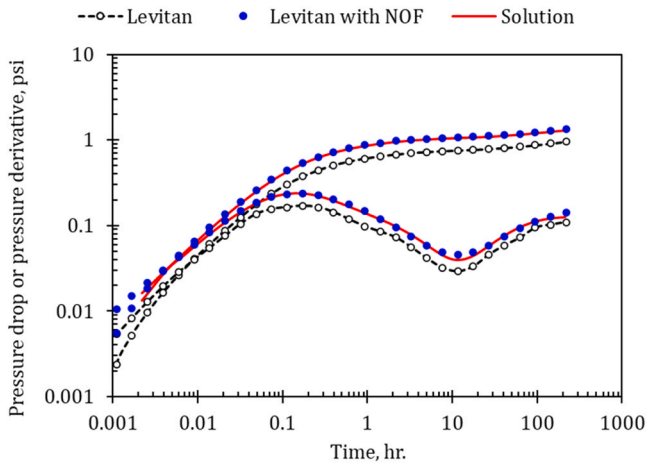

Fig. 11. Results from modified and original Levitan objective function – simulated example 2. Original is shifted; NOF reproduces the true pressure response.

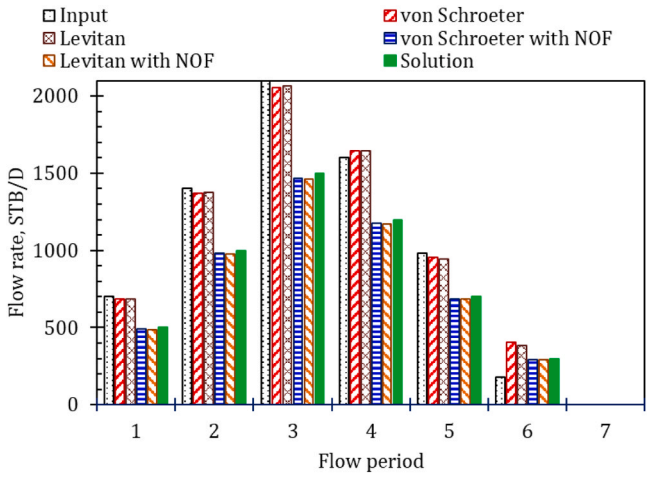

Fig. 12. Comparison of flow rates resulting from deconvolution with different techniques – simulated example 2. NOF recovers correct rates; originals remain biased.

Levitan with the original and new objective functions. In Fig. 7, the erroneous rates (blue line in Fig. 3) are shown as dotted columns, and the exact rates (red in Fig. 3) are given as green columns. The resultant rates from original von Schroeter and Levitan algorithms are shown in columns with red upward diagonals and brown diamond, respectively. von Schroeter and Levitan algorithms using the new objective function (NOF) result in rates demonstrated in columns with blue horizontal lines and dark orange downward diagonals, respectively. As is clearly seen from Fig. 7, the original objective functions forms are not able to adjust the rates to meet the true solution. However, the NOF proposed in this work recovers the correct flow rates.

4.2. *Simulated case 2*

The example is a 221-hour multi-rate test for a dual porosity reservoir of infinite-acting boundary. The noise level added to the data is 0.25 % for pressures (5469 points with errors of a standard deviation of 3.7 psi) and 40 % for rates. The initial pressure is treated as known in the cases presented in this section. The flow rate and pressure data are given in Figs. 8 and 9. von Schroeter and Levitan algorithms are implemented with the original and new objective functions. The results are given in Figs. 10–12. Investigating the results (Figs. 10 and 11) shows that the deconvolved pressure responses, with the original objective functions, are shifted below the correct solution. In addition, the results show downward pressure derivative trend at the end in Fig. 10, which can be wrongly interpreted as some boundary effects. The shifted pressure data can result in wrong permeability estimation. With the new objective function, the results are in good agreement with the right solution, and this is true for both deconvolution algorithms. Fig. 12 shows that the original objective functions are not able to correct the flow rates, while the new objective function completely recovers the correct rate values that match the right solution.

4.3. *Simulated case 3*

The data set is created for a 177-hour multi-rate test in a homogenous reservoir with no-flow boundary. The noise level added to the data is 0.1 % for pressures (2376 points with errors of 2.4 psi standard deviation) and 50 % for rates. The well test data are given in Figs. 13 and 14 for the flow rates and pressures, respectively. The deconvolution results are given in Figs. 15–16. Both von Schroeter and Levitan algorithms result in shifted pressure responses which are also distorted at the end as seen in Figs. 15 and 16. Applying the two algorithms using the original objective functions resulted in flow rates considerably different from the exact values. Using the same algorithms with the new objective function generates smooth

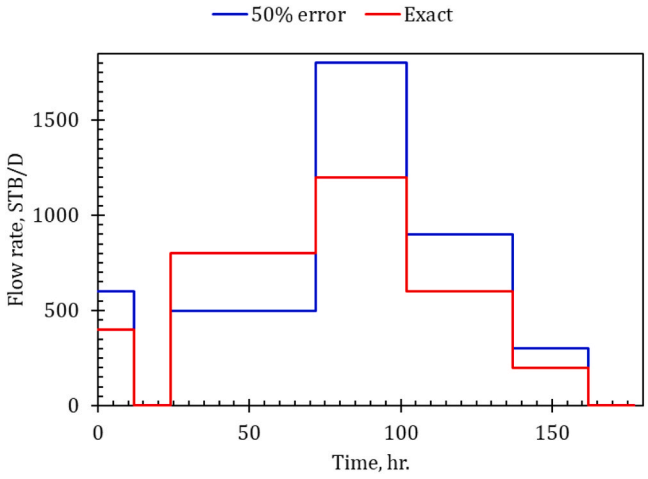

Fig. 13. Flow rate schedule – simulated example 3.

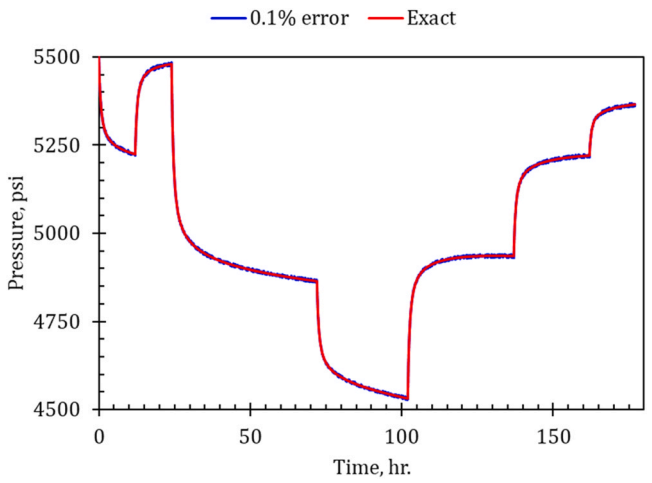

Fig. 14. Pressure profile – simulated example 3.

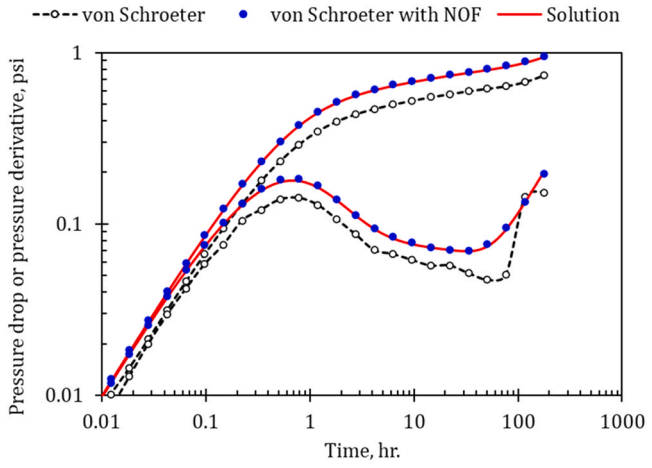

Fig. 15. Results from modified and original von Schroeter objective function – simulated example 3. Originals are shifted/distorted; NOF matches the true response.

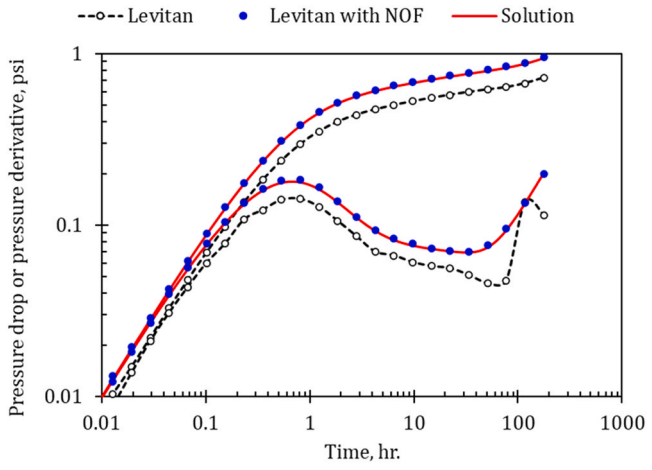

Fig. 16. Results from modified and original Levitan objective function – simulated example 3. Originals are shifted/distorted; NOF matches the true response.

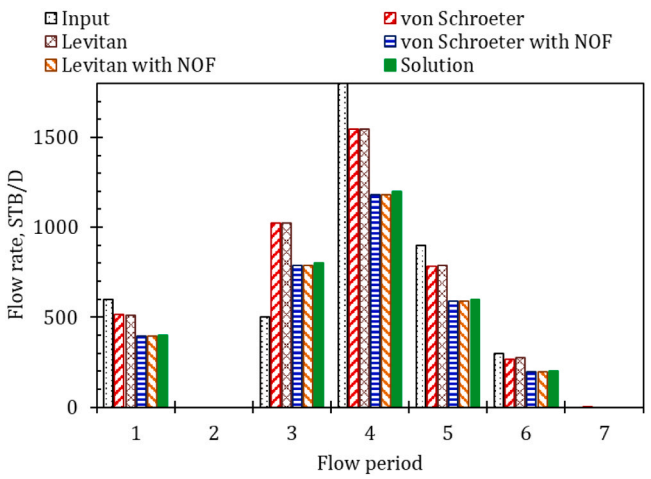

Fig. 17. Comparison of flow rates resulting from deconvolution with different techniques – simulated example 3. NOF corrects rates to true values; originals deviate.

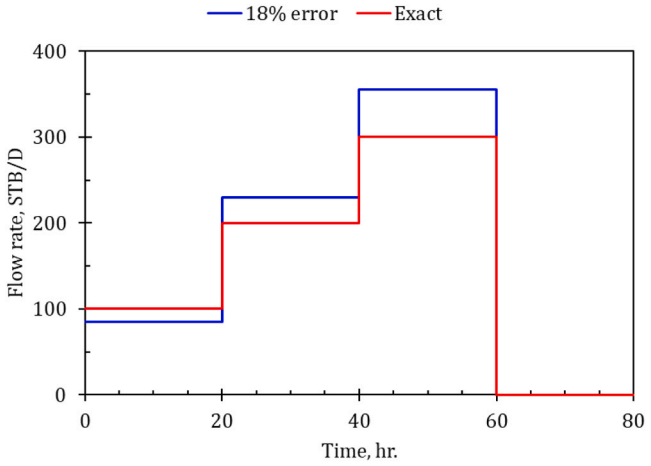

Fig. 18. Flow rate schedule – simulated example 4.

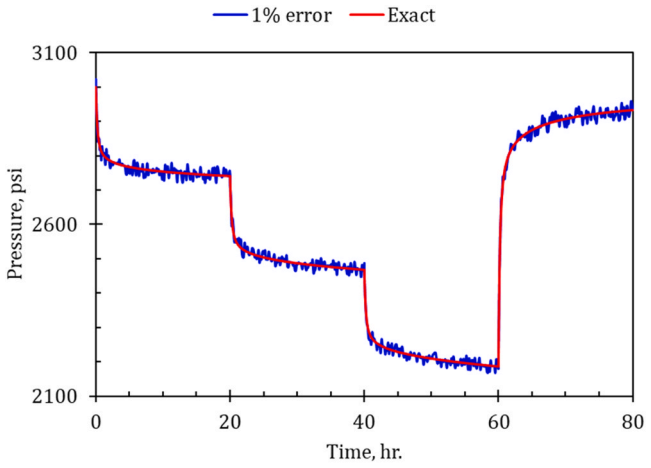

Fig. 19. Pressure profile – simulated example 4.

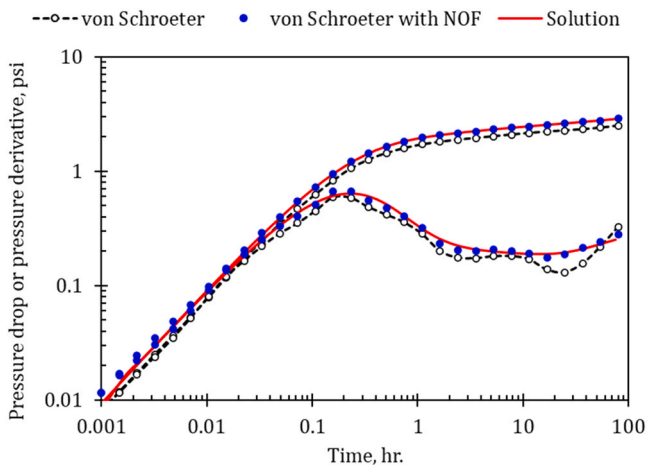

Fig. 20. Results from modified and original von Schroeter objective function – simulated example 4. NOF matches the solution; original deviates.

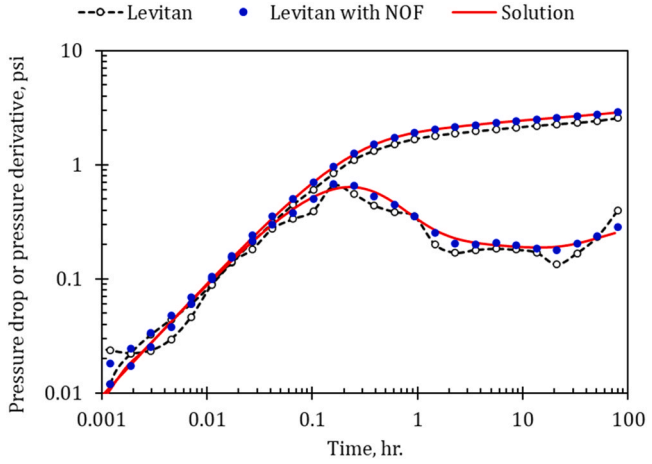

Fig. 21. Results from modified and original Levitan objective function – simulated example 4. NOF matches the solution; original deviates.

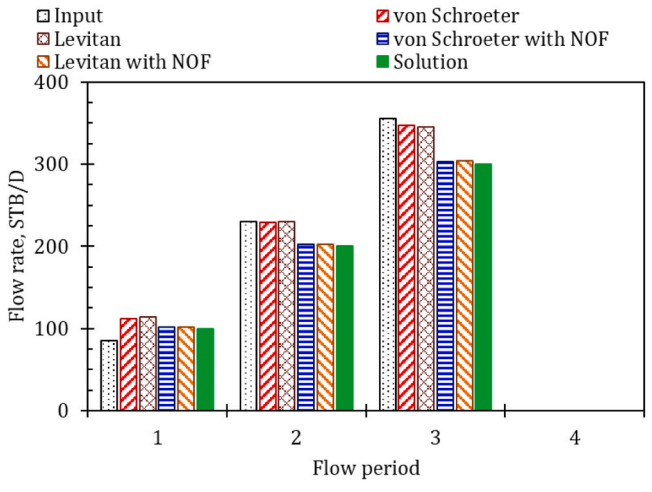

Fig. 22. Comparison of flow rates resulting from deconvolution with different techniques – simulated example 4. Originals overestimate; NOF adjusts to correct values.

pressure responses that matched the correct solution (Figs. 15 and 16) and modifies the flow rates to the correct values (Fig. 17).

4.4. Simulated case 4

The data set is an 80-hr test acquired from a vertical well in a homogenous reservoir with a fault. The noise levels introduced into this case are 1 % for the pressures (700 points with errors of a standard deviation of 12.2 psi) and 18 % for rates. The data sets are given in Figs. 18 and 19. The data set is processed with von Schroeter and Levitan algorithms with the original and modified objective functions. The results are presented in Figs. 20–22. In Figs. 20 and 21, the deconvolution pressure results from NOF meet the solution; however, the original objective functions show deviation from the exact results. In Fig. 22, the original objective functions overestimated the resultant flow rates. However, the NOF adjusted the rates to the correct values.

Quantitative evaluation of the deconvolved pressure drop results from von Schroeter and Levitan algorithms (with and without the NOF) was accomplished. The average deviation in pressure drop from the exact solution was computed for the cases. The comparison results (using MAPE, MAE, and RMSE) are listed in Table 3. As obvious from the table, the average errors from the NOF are much less than the errors when the original objective functions were used (with both von Schroeter and Levitan techniques). In the first example, the original von Schroeter objective function gives an average error of 37.4 % (MAPE); however, the same algorithm gives an average error of 8.4 % with the NOF. It can also be noticed that the deconvolution results from von Schroeter algorithm are better than Levitan algorithm. In the first case, von Schroeter with the NOF gave an average error around 8.4 %; however, Levitan with the NOF gave 27.6 % average error in the deconvolved pressure drop results.

5. Sensitivity analysis

This section presents a parametric analysis of the parameters G_P and G_q used in calculating NOF weights through Eqs. (11) and (12). Additionally, the implementation of deconvolution based on the Pimonov's methodology [33], employing von Schroeter and Levitan algorithms, is examined. The earlier examples did not adopt Pimonov's approach because it lacks a quantitative procedure to determine pressure and rate weights using explicit formulas or techniques. By contrast, von Schroeter et al. [5] and Levitan [6] proposed structured approaches for weight assignment. Pimonov et al. instead suggested qualitative guidance, recommending that weights between zero and one be assigned according to the reliability of measurements. For this reason, the present analysis applies those recommendations. A further limitation of Pimonov's methodology is the large number of weights that need to be manually defined for both pressure and rate data, which makes practical use challenging, as also highlighted by [11]. To address this, the current study allocates weights to pressure and rate data on a sectional basis (per flow period) rather than assigning distinct values for every single measurement.

A simulated drill stem test (DST) in a vertical well completed in a heterogeneous dual-permeability reservoir was generated to conduct the sensitivity analysis and apply Pimonov's objective function. The reservoir parameters are provided in Table 4, while the corresponding flow rate and pressure records are presented in Figs. 23 and 24. The positive skin values in this case represent wells with some near-wellbore damage. The total compressibility (c_t) reflects the combined effect of rock and fluid compressibility, typical of slightly compressible reservoirs. The oil formation volume factor (B_o) was set to 1.0 for simplicity, as B_o has no direct influence on the deconvolution calculations. Noise was

Table 3
Average error in the calculated deconvolved pressure drop signal as compared with the true values: Mean absolute percentage error (MAPE), mean absolute error (MAE), and root mean square error (RMSE).

	Example 1			Example 2			Example 3			Example 4		
	MAPE (%)	MAE (psi)	RMSE (psi)	MAPE (%)	MAE (psi)	RMSE (psi)	MAPE (%)	MAE (psi)	RMSE (psi)	MAPE (%)	MAE (psi)	RMSE (psi)
von Schroeter	37.4	0.121	0.154	27.8	0.171	0.211	20.0	0.076	0.105	14.1	0.175	0.227
von Schroeter with NOF	8.4	0.007	0.008	2.1	0.013	0.017	3.3	0.006	0.009	4.2	0.012	0.014
Levitan	53.6	0.135	0.167	32.3	0.158	0.203	20.1	0.068	0.100	12.0	0.148	0.202
Levitan with NOF	27.6	0.014	0.016	4.9	0.017	0.020	7.0	0.006	0.008	6.3	0.011	0.014

Table 4
Properties of parametric study example – DST.

p_i (psi)	B_o (STB/bbl)	μ_o (cp)	k (md)	h (ft)	WBS Coeff. (bbl/psi)
5000	1.0	5	90	60	0.0015
Skin	**Skin2**	**Porosity**	**c_t (psi^{-1})**	**Omega**	**Lambda**	**Kappa**
0.8	1	15 %	3E−06	0.25	8E−7	0.99

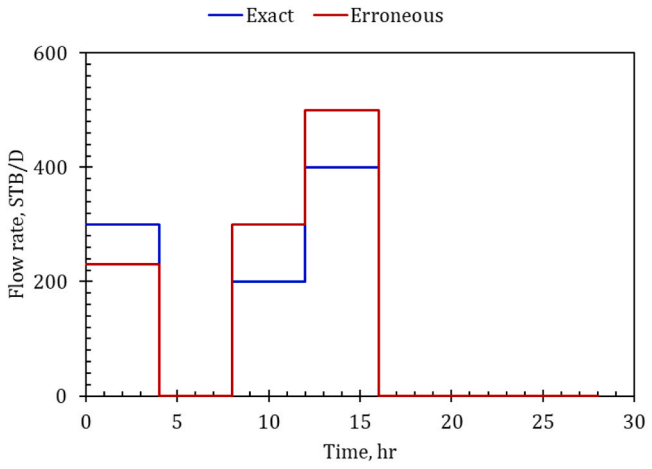

Fig. 23. Flow rate schedule – DST.

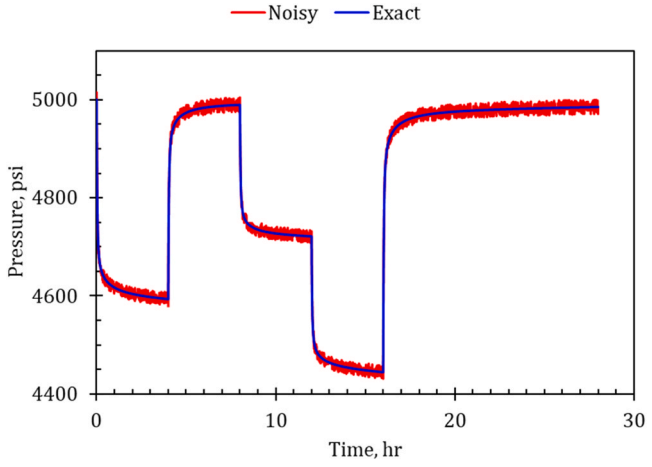

Fig. 24. Wellbore pressure signal – DST.

introduced into the test data at levels of 0.3 % for pressures ($G_P = 0.003$) and 50 % for rates ($G_q = 0.5$). The parametric evaluation was carried out using the modified objective function combined with the von Schroeter deconvolution algorithm, treating the initial reservoir pressure as an unknown variable to demonstrate that the deconvolution can verify or

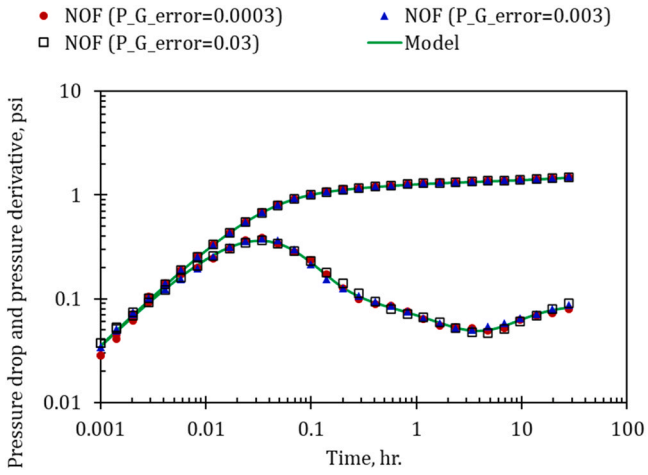

Fig. 25. Results from modified objective function - sensitivity on G_P – DST. Deconvolved pressure aligns with the true response across 0.03 %-3.00 %.

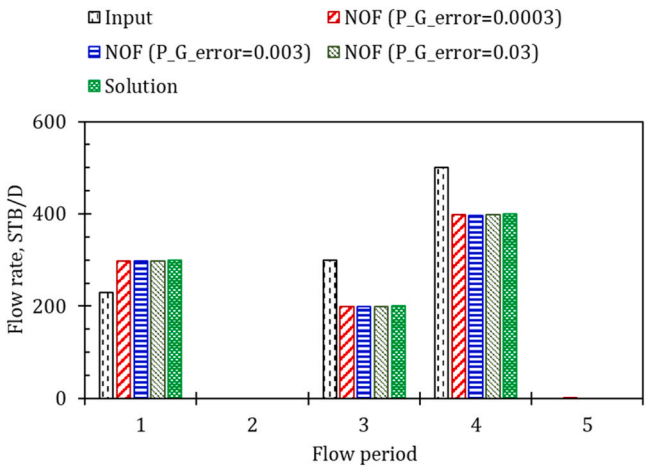

Fig. 26. Comparison of flow rates resulting from modified objective function - sensitivity on G_P value – DST. NOF reproduces flow rates across 0.03 %-3.00 %.

Table 5
Sensitivity on G_P - MAPE error in the deconvolved pressure signal along with the estimated initial pressure and the required smoothing parameter (Lambda) – DST.

G_P (%)	Error in pressure drop (%)	Error in pressure derivative (%)	Lambda	p_i (psi)
0.03	2.3	5.1	1.00E+ 04	5000
0.3	1.2	4.2	1.78E+ 03	5000
3	1.3	3.3	3.16E+ 02	4999

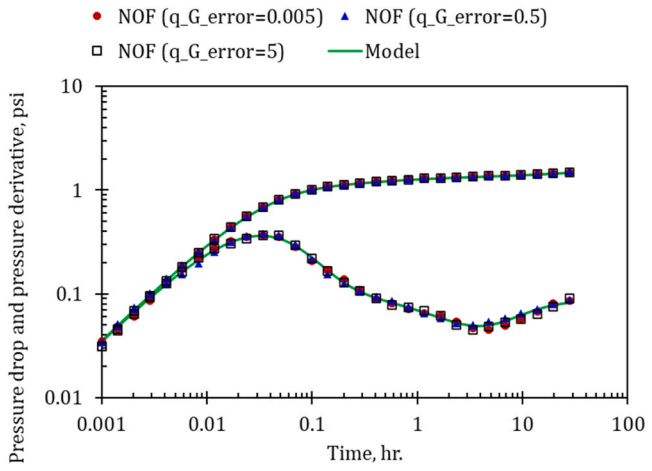

Fig. 27. Results from modified objective function - sensitivity on G_q – DST. Deconvolved pressure remains aligned with the true response across 0.5 %-500.0 %.

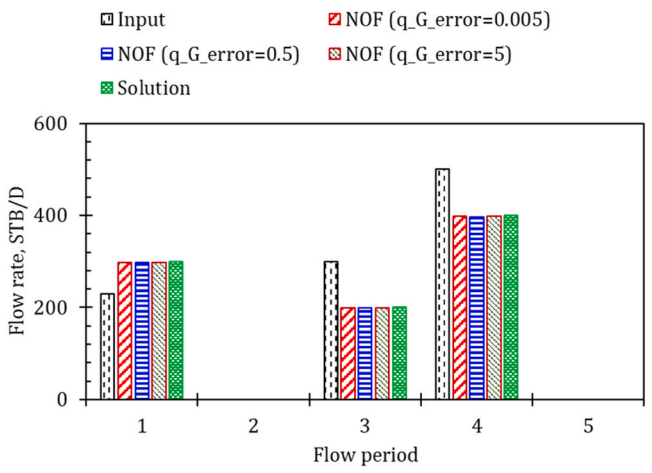

Fig. 28. Comparison of flow rates resulting from modified objective function - sensitivity on G_q – DST. NOF reproduces flow rates across 0.5 %-500.0 %.

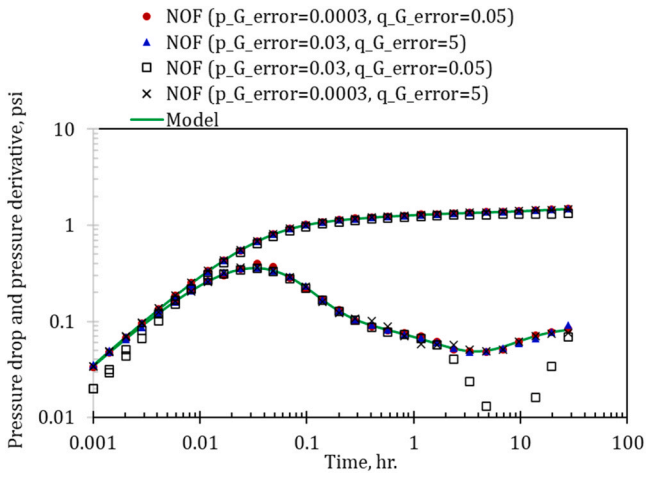

Fig. 29. Results from modified objective function - sensitivity on G_P and G_q – DST.

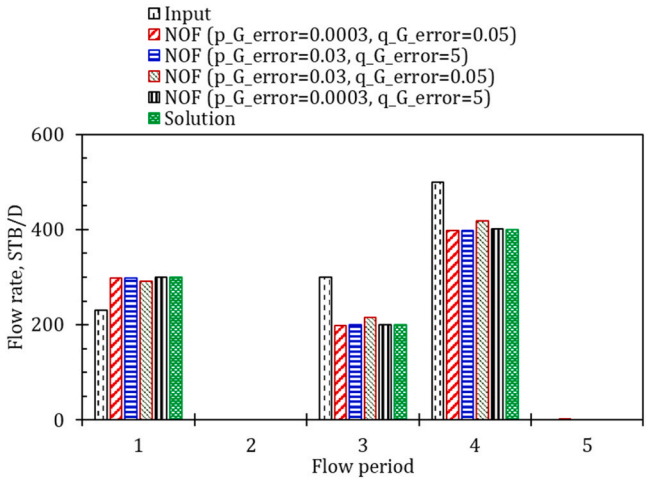

Fig. 30. Comparison of flow rates resulting from modified objective function - sensitivity on G_P and G_q – DST.

Table 6
Sensitivity on G_q - MAPE error in the deconvolved pressure signal along with the estimated initial pressure and the required smoothing parameter (Lambda) – DST.

G_q (%)	Error in pressure drop (%)	Error in pressure derivative (%)	Lambda	p_i (psi)
0.5	0.9	4.2	1.00E+ 03	4999
50	1.2	4.2	1.78E+ 03	5000
500	1.5	4.2	1.00E+ 03	4999

Table 7
Sensitivity on G_P and G_q - MAPE error in the deconvolved pressure signal along with the estimated initial pressure and the required smoothing parameter (Lambda) – DST.

G_P (%)	G_q (%)	Error in pressure drop (%)	Error in pressure derivative (%)	Lambda	p_i (psi)
0.03	5	0.8	2.9	1.00E+ 04	4999
3	500	0.5	2.5	1.78E+ 02	4999
3	5	11.3	20.7	3.16E+ 02	4987
0.03	500	0.6	3.9	1.00E+ 04	4999

recover it from the available data, although the initial pressure is normally measured in DST operations.

The sensitivity analysis on G_P was carried out over a wide interval ranging from 0.03 % to 3 %, while maintaining G_q fixed at 50 %. Weights for both pressure and rate measurements were assigned according to Eqs. (11) and (12). The NOF was applied using the von Schroeter algorithm, with the outcomes presented in Fig. 25 for the constant-rate pressure response and in Fig. 26 for the corresponding flow rates. Fig. 25 demonstrates that the deconvolved pressure profiles align closely with the exact solution. Likewise, Fig. 26 shows that the NOF successfully reproduces the flow rates across the entire investigated range of G_P. Quantitative assessment of the mean errors in deconvolved pressure drop and pressure derivative is summarized in Table 5, together with the estimated initial pressure and smoothing parameter (Lambda). The results indicate smaller errors in pressure drop compared to pressure derivative, and confirm that the NOF accurately recovers the initial pressure of 5000 psi. This outcome is expected, as smaller errors in pressure drop compared to pressure derivative are typical for stable deconvolution results.

The impact of G_q on the NOF, as defined in Eq. (12), was analyzed across a range extending from 5 % to 500 %, while maintaining G_P constant at 0.3 %. Application of the NOF using the von Schroeter algorithm produced the outcomes shown in Figs. 27 and 28. These results

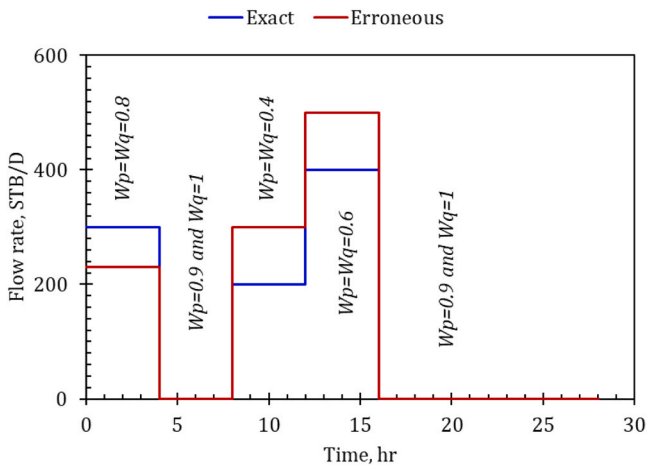

Fig. 31. Weights (based on section) for Pimonov Implementation – DST.

demonstrate that the deconvolved pressure and rate responses align with the true solution. Table 6 provides a quantitative assessment of the associated errors together with the estimated initial pressures. The error magnitudes listed in this table are comparable to those reported in Table 5. Based on the sensitivity results for G_P (Figs. 25 and 26) and G_q (Figs. 27 and 28), modifying one parameter while holding the other at its correct value (0.3 % for pressure and 50 % for rate) does not introduce bias into the deconvolution outcomes. Varying G_q, in Table 6, across two orders of magnitude produced minor change in the pressure-drop and derivative errors. This outcome indicates that the deconvolution results are primarily controlled by pressure-measurement accuracy (G_p), while rate accuracy (G_q) has a minor effect.

The simultaneous variation of G_P and G_q was investigated by applying the NOF procedure, with results shown in Figs. 29 and 30. When both parameters were altered in the same direction (either overestimated or underestimated), the quality of the resulting pressure signals and flow rates was not significantly impacted. In contrast, Fig. 29 illustrates that substantial deviation from the correct solution occurred when G_P was set to 0.03 and G_q to 0.05, representing the scenario of overestimated G_P and underestimated G_q. In this situation, the parameters were adjusted in opposite directions. Fig. 30 further indicates that the corresponding flow rates retained noticeable errors. The estimated initial pressure in this case (Table 7) was underestimated by 13 psi. This behavior may be attributed to the larger value of G_P driving considerable adjustments in the measured pressures (serving as inputs), while the smaller G_q limited changes in flow rates, which act both as measured

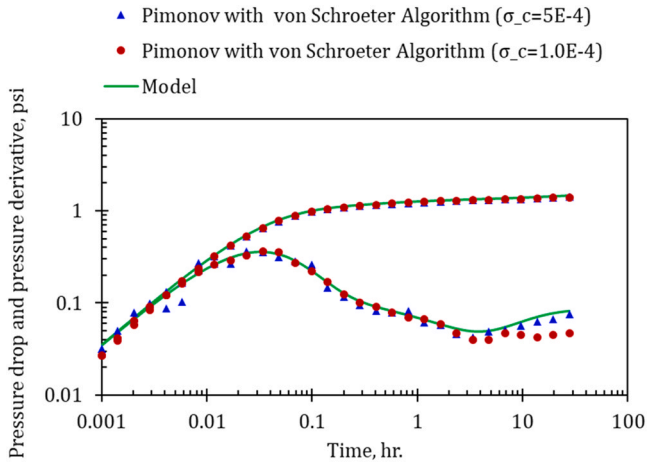

Fig. 32. Results from Pimonov Objective Function with von Schroeter Algorithm – DST.

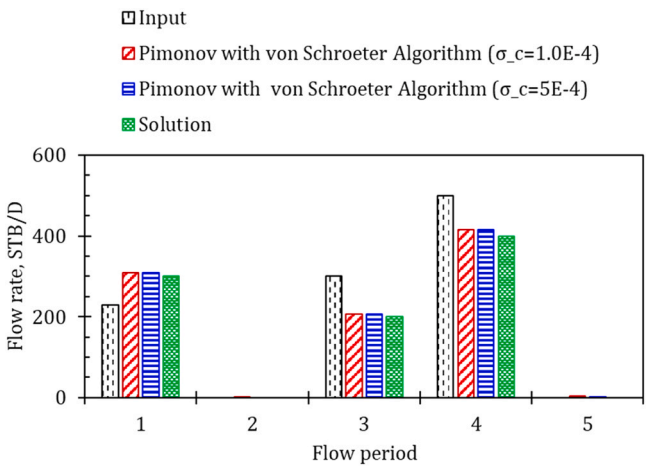

Fig. 33. Comparison of flow rates resulting from Pimonov Objective Function with von Schroeter Algorithm – DST.

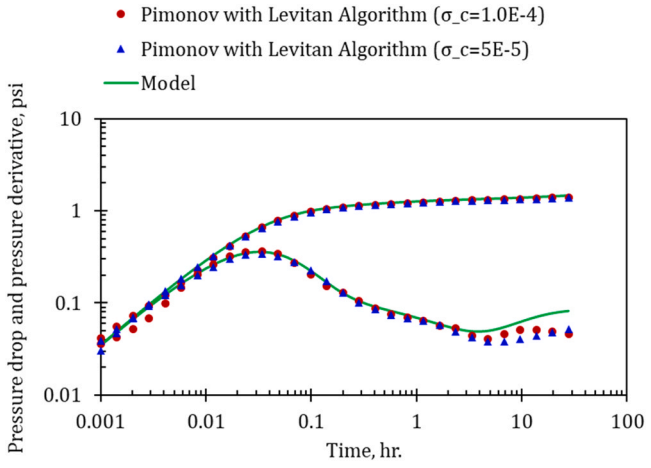

Fig. 34. Results from Pimonov Objective Function with Levitan Algorithm – DST.

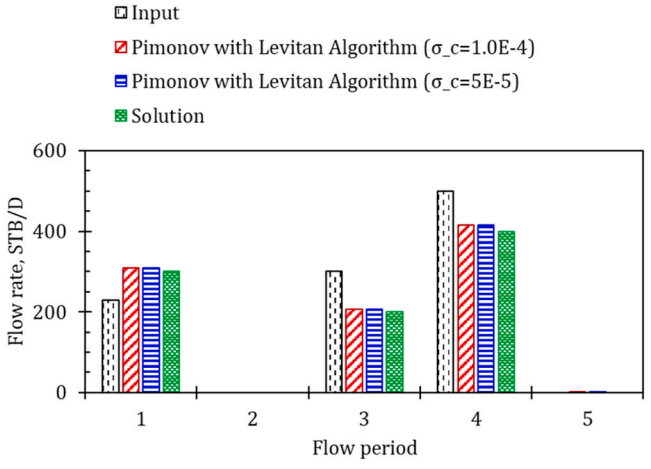

Fig. 35. Comparison of flow rates resulting from Pimonov Objective Function with Levitan Algorithm – DST.

inputs and corrected outputs during optimization. As illustrated in Fig. 30, only minimal corrections were applied to the flow rates due to their greater restriction compared to pressures. Conversely, when G_q was set at 500 % (overestimated) and G_P at 0.03 % (underestimated), the deconvolution produced accurate pressure and flow rate results.

Table 8
Pimonov objective function with von Schroeter and Levitan algorithms - MAPE error in the deconvolved pressure signal along with the estimated initial pressure – DST.

	Error in pressure drop (%)	Error in pressure derivative (%)	Estimated p_i (psi)
von Schroeter (σ_c=1.00E−4)	5.9	12.7	4999
von Schroeter (σ_c=5.00E−4)	4.5	13.2	4998
Levitan (σ_c=1.00E−4)	6.2	15.0	4997
Levitan (σ_c=5.00E−5)	8.2	12.3	4996

Table 9
The NOF with Levitan algorithm - MAPE error in the deconvolved pressure signal along with the estimated initial pressure – DST.

Error in pressure drop (%)	Error in pressure derivative (%)	Estimated p_i (psi)
3.1	3.4	5001

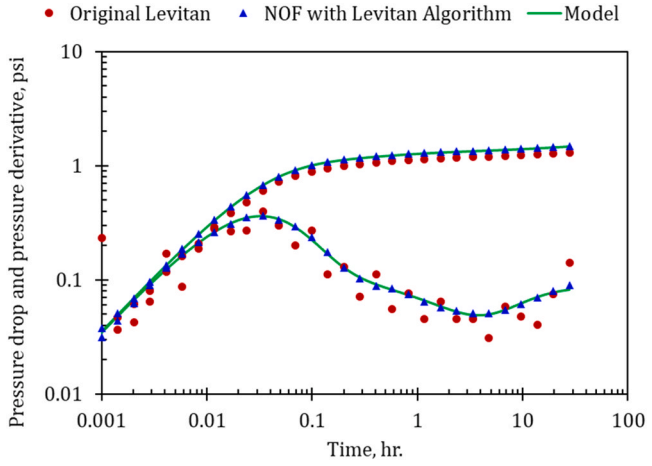

Fig. 36. Results from modified objective function with Levitan Algorithm – DST.

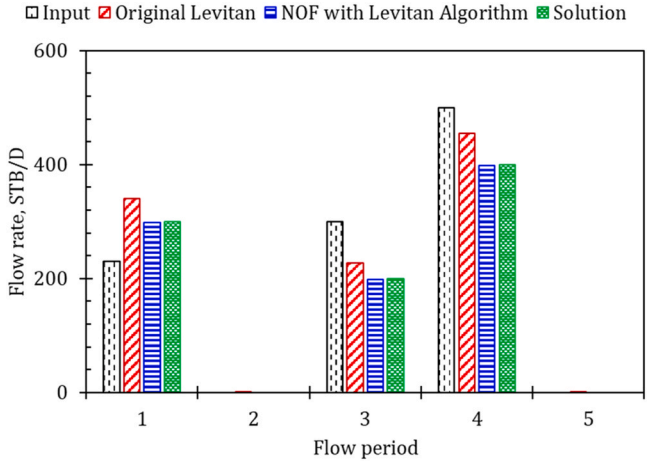

Fig. 37. Comparison of flow rates resulting from modified objective function with Levitan Algorithm – DST.

Table 10
Basic properties of the field case.

h (ft)	ϕ (%)	B_o (bbl/STB)	μ (cp)	C_t (psi^{-1})	r_w (ft)	p_i (psi)
20	8	1.3	1.3	5.0×10^{-6}	0.29	7843

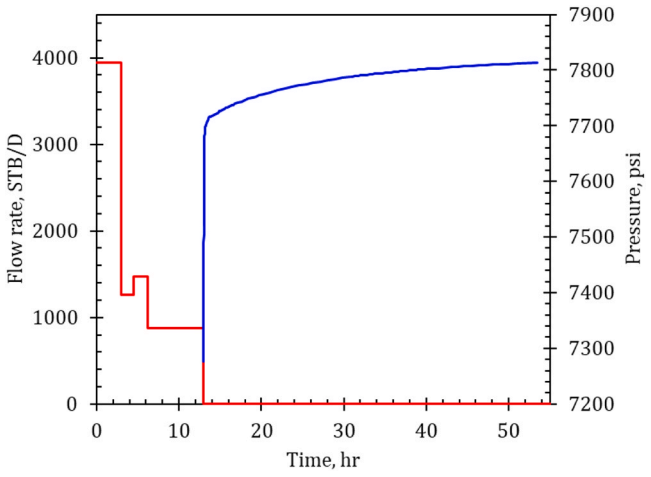

Fig. 38. Pressure and rate measurements (variable-rate drawdown and buildup) - field case study.

Under these conditions, the flow rates, as the primary outputs, had sufficient flexibility to adjust, while the pressures, as inputs, were more constrained. This increased flexibility in flow rates explains the successful correction. Quantitative error estimates for these scenarios are summarized in Table 7, along with the recovered initial pressures and the required smoothing parameter.

From this sensitivity study, the qualities of results (flow rates, constant-rate pressure signal and initial pressure) are related. Therefore, introducing more flexibility on flow rates (G_q) is favorable to allow obtaining corrected results. Here, flexibility in G_q refers to the tolerance assigned to rate-measurement uncertainty within the optimization process.

For the implementation of the Pimonov approach (Eq. (9)), no explicit procedure or equations were provided to assign detailed weights to pressure and rate measurements. In this study, weights (W_p^i, W_q^j) for pressures and rates were assigned by test section (flowing or shut-in) rather than for individual data points. Following Pimonov's approach, the weights were restricted between zero and one, as shown in Fig. 31.

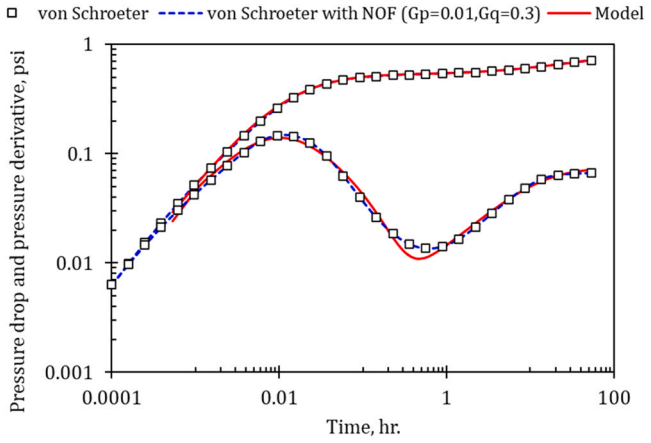

Fig. 39. Deconvolution results from von Schroter algorithm for the field case.

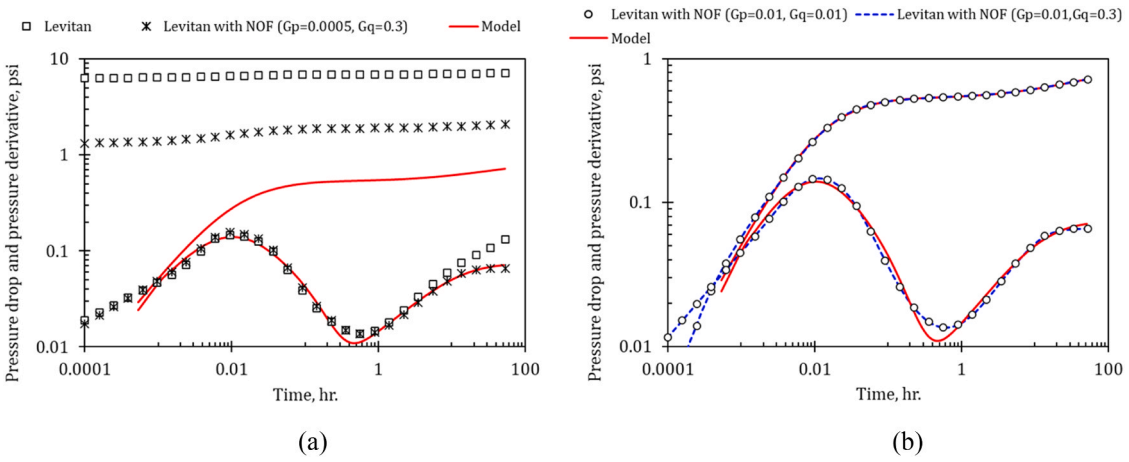

Fig. 40. Deconvolution results from Levitan algorithm for the field case: Levitan without NOF, and Levitan with NOF (G_p=0.05 %, G_q=30 %) (a), and Levitan with NOF for (G_p=1 %, G_q=1 %) and (G_p=0.1 %, G_q=30 %) (b) along with the solution model (in red).

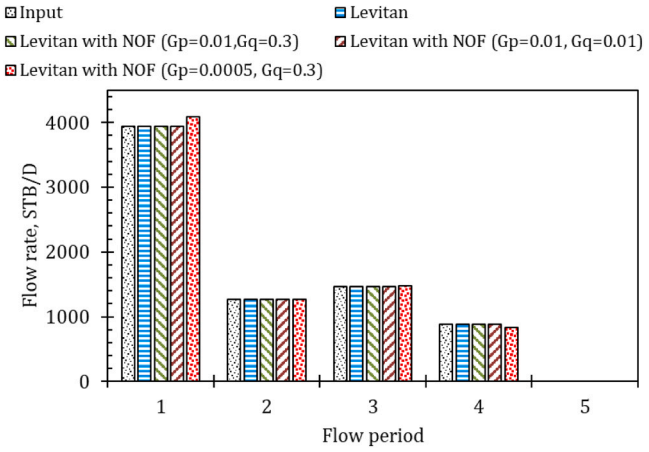

Fig. 41. Rate results from Levitan algorithm for the field case. Reconstructed rates closely match the measured input schedule.

The error bounds σ_p and σ_q in Eq. (9) were fixed at 0.003 for pressures and 0.5 for rates. The Pimonov methodology was applied using both von Schroeter and Levitan algorithms, with results shown in Figs. 32 and 33 for two smoothing parameter values, σ_c. The deconvolved pressure signals and flow rates aligned reasonably with the solution; however, the Levitan implementation (Figs. 34 and 35) displayed end-of-test deviations. A comparison revealed that the Pimonov function performed better with von Schroeter. Quantitative error estimates are summarized in Table 8. For comparison, the NOF was also applied to the DST with Levitan (Table 9; Figs. 36 and 37), showing strong performance consistent with results from von Schroeter (Figs. 25 and 26).

6. Field case application

To demonstrate the applicability of the proposed measurement-driven objective function, a well test originally published by [44] was revisited. The dataset comprises a multi-rate drawdown sequence followed by a buildup test in a heterogeneous reservoir. Only shut-in pressure readings and the complete production history were available, making this case representative of the practical limitations often encountered in field operations. The basic reservoir and fluid properties are summarized in Table 10. The listed total compressibility (c_t) accounts for both rock and fluid contributions, representing the total system compressibility.

The test consisted of approximately 13 h of variable-rate drawdown, followed by 40.4 h of buildup (Fig. 38). The data were analyzed using both conventional deconvolution approaches and the proposed noise-oriented function (NOF), embedded within the von Schroeter and Levitan algorithms. This setup enabled a direct comparison with standard practices under realistic field conditions.

Table 12
Error metrics across the tested pairs for the field-case. For the final interpretation, G_p = 0.01 and G_q = 0.3 were selected.

Algorithm	Signal	RMSE (psi)	MAE (psi)	MAPE (%)
von Schroeter	pressure derivative	0.0039	0.0034	1.4
von Schroeter	pressure drop	0.0044	0.0034	7.3
von Schroeter with NOF (G_p=0.01, G_q=0.3)	pressure derivative	0.0039	0.0034	1.4
von Schroeter with NOF (G_p=0.01, G_q=0.3)	pressure drop	0.0044	0.0034	7.3
von Schroeter with NOF (G_p=0.01, G_q=0.05)	pressure derivative	0.0040	0.0035	1.4
von Schroeter with NOF (G_p=0.01, G_q=0.05)	pressure drop	0.0044	0.0034	7.3
Levitan	pressure derivative	6.3556	6.3555	3141.6
Levitan	pressure drop	0.0120	0.0083	16.1
Levitan with NOF (G_p=0.01, G_q=0.3)	pressure derivative	0.0028	0.0022	1.8
Levitan with NOF (G_p=0.01, G_q=0.3)	pressure drop	0.0046	0.0035	7.7
Levitan with NOF (G_p=0.01, G_q=0.01)	pressure derivative	0.0027	0.0021	1.8
Levitan with NOF (G_p=0.01, G_q=0.01)	pressure drop	0.0046	0.0035	7.7
Levitan with NOF (G_p=0.0005, G_q=0.3)	pressure derivative	1.3539	1.3539	665.0
Levitan with NOF (G_p=0.0005, G_q=0.3)	pressure drop	0.0070	0.0050	9.4

Table 11
Solution of the field case.

Reservoir Model	Boundary	k (md)	Skin1	Skin2	Omega	Lambda	Kappa
Two layers	Infinite	87.2	−3.88	−2.56	0.01	2.18×10^{-7}	0.924

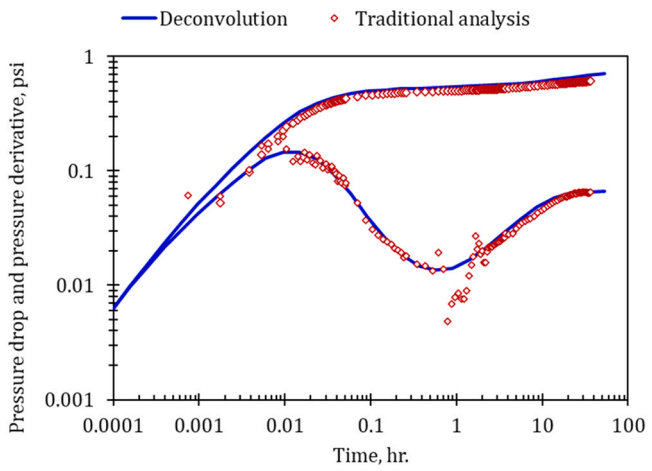

Fig. 42. Analysis comparison of deconvolution and traditional method for the field case. Deconvolution extends the interpretation window and yields a smoother derivative over the full 53.4-hr test.

Table 13
Summary of selected noise levels (G_p, G_q) and corresponding smoothing parameter λ for simulated cases, DST best selection, and field best selection. The DST sensitivity analysis was carried out using the von Schroeter algorithm.

Case	G_p (%)	G_q (%)	λ (von Schroeter, NOF)	λ (Levitan, NOF)
Simulated case 1	0.5	33	1.0×10^3	1.0×10^3
Simulated case 2	0.25	40	3.2×10^3	5.6×10^3
Simulated Case 3	0.1	50	3.2×10^3	5.6×10^3
Simulated case 4	1.0	18	7.5×10^2	5.6×10^2
DST case (sensitivity analysis)	0.3	50	1.78×10^3	-
Field case	1.0	30	3.16×10^2	3.16×10^2

Deconvolution with the von Schroeter formulation was applied to both the conventional method and the NOF-based approach. Since gauge specifications were not reported in [44], a sensitivity analysis was performed on (0.05 % and 1 %) and (5 % and 30 %) within the NOF framework. Both the original and NOF-enhanced approaches reproduced consistent pressure responses (Fig. 39). Only one representative case (G_p = 0.01, G_q = 0.3) is shown, as the remaining cases yielded similar results. The reconstructed rate history from the tested scenarios closely matched the original input schedule.

Integration of the NOF into the Levitan algorithm (Figs. 40 and 41) further demonstrated its robustness. Sensitivity analysis on G_p (0.05 % and 1 %) and G_q (5 % and 30 %) was conducted, comparing the NOF-based approach against the traditional Levitan formulation. The conventional Levitan method yielded unrealistic pressure-drop behavior (significant pressure changes under a production rate of 1 STB/D). In contrast, the NOF approach improved stability and accuracy, with reasonable results observed for the cases (G_p= 0.01, G_q= 0.01) and (G_p= 0.01, G_q= 0.3). The results were particularly sensitive to G_p, while G_q values of 0.05 and 0.3 consistently produced reliable outcomes. This aligns with the reconstructed rates in Fig. 41, where the NOF-derived rates matched closely with the measured input schedule. The resulting reservoir model corresponds to a two-layer system with infinite-acting boundary conditions, permeability of 87.2 md, and negative skin factors of −3.88 and −2.56 (Table 11). The two negative skin values correspond to the two-layer reservoir and indicate that both layers represent stimulated conditions. For the field case, G_p = 0.01 and G_q = 0.3 were selected for the final interpretation; comparative error metrics for all tested pairs are reported in Table 12.

Fig. 42 compares the deconvolution results (von Schroeter formulation, Fig. 39) with those obtained from traditional buildup analysis. The deconvolved pressure response provides smooth extension over the entire test duration (53.4 h), overcoming the limitations of the buildup-only approach (restricted to 40.4 h and scattered due to noise in pressure measurements). This highlights the advantages of deconvolution in extending the interpretation window and reducing the dependency on superposition assumptions in pressure transient analysis. To make it easy for readers to locate all parameter settings, Table 13 compiles every λ value and (G_p, G_q) pair used in the simulated cases and the field application.

7. Discussion

von Schroeter objective function includes two weighting parameters (ν and λ). Two equations were previously presented to estimate these parameters. The equations do not guarantee optimum estimate for their values. The authors used the value of λ from the proposed equation (Eq. (6)) as initial guess. The value is then modified manually until obtaining smooth deconvolved pressure derivative. Levitan presented three weighting parameters (σ_p, σ_q, and σ_c) in the objective function. Levitan used pressure gauge resolution and 0.05 for σ_p and σ_c, respectively. Levitan stated that σ_q is set subjectively based on the error in rate measurements. Pimonov objective function proposed five weighting parameters (σ_p, σ_q, σ_c, $w_{p_i}$and w_{q_i}) with $w_{p_i}$and w_{q_i} are sets of values. Initial estimations of 0.01 and 10 were proposed for σ_p and σ_q, respectively. The two values are then adjusted subjectively until smooth well test derivative is obtained. Pimonov et al. (2010) does not provide an approach to change these two parameters to obtain the smooth deconvolution derivative. Quantities between zero and one for $w_{p_i}$and w_{q_i} are chosen manually. Pimonov et al. (2010) does not offer a mechanism to select specific values for these parameters. In addition, it is practically difficult to manually adapt different weights to each point of pressure and rate measurements, as discussed by Cumming et al. (2013). Pimonov objective function uses a value of 0.05 for σ_c. The objective function proposed in this work includes three weighting parameters only. Eqs. (11) and (12) present objective estimations for two parameters ($w_{p_i}$and w_{q_i}). The third parameter (λ) is specified subjectively (following von Schroeter approach) until a smooth deconvolved signal is obtained.

The examples presented in this work show that the value of smoothing/curvature parameter (λ for von Schroeter and σ_q for Levitan) varies from one case to another. This observation confirms the recommendation given by von Schroeter at al. to use Eq. (6) for initial estimate and changing it subjectively until smooth deconvolution results are obtained. In addition, Pimonov et al. (2010) recommend to adjust the two parameters σ_p and σ_q to obtain smooth deconvolved well test derivative. This means that the values suggested by Levitan do not always give good results.

The new objective function reduces/simplifies the multiple weighting values to one weight. For example, Pimonov objective function uses $\frac{1}{2}$, w_{q_j} and σ_q as weights in the rate term while these three weights are reduced to one weight w_{qj} in the new objective function. In addition, the flow rate regularization parameter (ν) given in von Schroeter objective function is excluded. von Schroeter et al. presented an expression to evaluate this parameter; however, the expression did not guarantee optimum estimation of the parameter. von Schroeter et al. stated that the estimation of the flow rate weight parameter remained as an unresolved problem that should be tackled in future work.

The new objective function employs an automated technique to specify the weights of the many pressure and rate measured data points. The strategy of setting these weights is to equalize the contributions of the different well test measurements in the error/residue of optimization. Therefore, the implementation of this strategy takes the gauge accuracy into consideration. The accuracy of the gauge is often available from the gauge manufacturer.

Analysis of the simulated cases indicates a clear, negative relationship between λ and pressure error level. As the pressure accuracy de-

creases (i.e., error increases), the selected λ systematically decreases, reflecting the need for less smoothing under higher noise conditions. In contrast, rate error shows only a weak and non-monotonic effect on λ. This trend holds consistently across all simulated examples, confirming that λ is primarily governed by pressure measurement accuracy. This supports that the parameter selection is guided rather than completely subjective.

In real field work, this study helps engineers choose gauge parameters with confidence. The pressure weight should match the gauge real accuracy because results are more sensitive to pressure than to flow rate. The rate term can be more flexible since rate data are usually less accurate. If the pressure weight is set too high or the rate weight too low, the pressure response may shift slightly. Using realistic pressure accuracy (about 0.05 %–1.00 %) and reasonable rate accuracy (about 5 %–50 %, depending on how it is measured) gives stable results. In practice, engineers should rely on the manufacturer accuracy for pressure gauges and apply cautious ranges for rate measurements. With this approach, the NOF method provides smooth, accurate, and reliable performance in real field applications.

This study also has broader implications for practical well test analysis. The NOF approach can be directly integrated into commercial well-testing software because it only modifies the objective function structure without changing the deconvolution workflow. This allows automatic weighting and smoother responses with minimal user input. In terms of computation, the NOF adds only a small cost since the additional steps involve simple iterative weight adjustments, which are negligible compared with full deconvolution or inversion runs. The method therefore remains suitable for real-time analysis and field applications. Nonetheless, as with any data-driven optimization, results may still depend on data quality, gauge calibration, and stability of rate measurements.

In the simulated examples, Case 1 assumes a homogeneous, infinite-acting reservoir with $P_i = 5000$ psi; Case 2 adopts a dual-porosity, infinite-acting system with $P_i = 4000$ psi; Case 3 represents a homogeneous reservoir with a no-flow circular boundary and $P_i = 5500$ psi; and Case 4 models a homogeneous reservoir intersected by a single fault with $P_i = 3000$ psi (Table 1). These cases cover a wide range of typical initial and boundary conditions of field cases. For the field case, the interpreted system is a two-layer reservoir under infinite-acting boundary conditions, with $P_i = 7843$ psi (Table 10).

Typical failure modes include oscillatory or noisy deconvolved signals, or late-time drift in pressure. These artifacts generally indicate under-smoothing (small λ) or unrealistic accuracy settings (e.g., tight G_p). Increasing λ from its initial estimate (Eq. (6)) until the derivative is smooth but still responsive, and using realistic accuracy ranges, resolves most issues. Sensitivity tests also showed that using opposite-direction settings for G_p and G_q can introduce bias in results; keeping both consistent with instrument specifications avoids this effect.

The pressure- and rate-accuracy inputs (G_p, G_q) that define the NOF weights (Eqs. (11) and (12)) translate measurement precision directly into the relative influence of each data stream on the optimized solution. The parametric results show that deconvolved pressure accuracy is governed primarily by pressure-measurement accuracy, with rate accuracy exerting a weaker, second-order effect (Tables 5–7; Figs. 25–30). Accordingly, uncertainty bands for the deconvolved signal contract when G_p improves.

When p_i is not provided, it is treated as a free parameter within the pressure-match term of the objective (Eq. (10)). In the Levitan formulation, the first-node pressure drop is estimated as an explicit unknown (Eq. (7)). The smoothing weight λ controls only the curvature (smoothness) term and is not directly affected by p_i.

In all examples and the field case, pressure and rate were recorded with aligned timestamps, so no time-shift correction was required. For datasets where alignment is uncertain, a simple visual check of rate changes against corresponding pressure responses is recommended before deconvolution.

The manufacturer accuracy is used to set per-sample errors in Eqs. (11) and (12). When specifications are not available, the ranges used in this study can be used for guidance. For downhole pressure readings, the available technology commonly reads $G_p \leq 1$ %. For flow rate, $G_q = 5$ %–30 % for routine tests, and higher when rates are poorly constrained (e.g., tank/choke setups). These defaults were used/validated in this study simulations and field sensitivity.

All example and field-case runs were executed on a standard personal workstation (Intel i7-10750H, 16 GB RAM, Windows 11, MATLAB R2025a). Each complete deconvolution, including the NOF term, required only a few seconds. The added NOF term therefore introduces only minimal overhead relative to the original objective. For this study von Schroeter runs, variable projection was used with MATLAB function "lsqnonlin" and an analytic Jacobian; no line search was invoked. For Levitan runs, "lsqnonlin" with the "Levenberg-Marquardt" MATLAB algorithm and an analytic Jacobian was used; no line search was invoked. Convergence tolerances and maximum iterations were left at MATLAB defaults.

8. Conclusion

This study introduced a new measurement-driven objective function (NOF) for well test deconvolution. The function eliminates the subjectivity inherent in earlier formulations by assigning automated weights to pressure and rate data based on gauge accuracy. This approach normalizes the contributions of different measurements, simplifies weighting to a single parameter per term, and excludes the unresolved flow rate regularization parameter present in previous methods.

Application to multiple simulated cases demonstrated that the NOF consistently produced more accurate pressure responses and corrected flow rates, even under high noise levels, compared to von Schroeter, Levitan, and Pimonov objective functions. Quantitative evaluation confirmed that the NOF reduced average deconvolution errors significantly across all tested scenarios. Sensitivity analysis showed that the method is robust to variations in specified measurement accuracy. In addition, the field case application further validated the robustness and practicality of the NOF. Unlike conventional formulations, the NOF improved stability, matched production history, and yielded reservoir parameters consistent with physical expectations.

The NOF offers an automated and practical method for weighting well test measurements. It enhances the accuracy, stability, and reliability of deconvolution, and can be readily implemented within existing stable deconvolution algorithms, providing a stronger basis for pressure transient analysis and reservoir characterization.

Nomenclature

B_o: Oil formation volume factor, bbl /STB
C_t: Total compressibility, psi^{-1}
$\widetilde{C}(z)$: Design matrix of pressure match (Levitan Eq. (8))
$C(z)$: Design matrix of pressure match (von Schroeter Eq. (5))
D: Constant matrix in curvature term (von Schroeter Eq. (5), and Levitan Eq. (8))
$g\,(t)$: Derivative of constant rate pressure drop function, psi/hr
G_P: Error level in pressure gauge, fraction
G_q: Error level in rate gauge, fraction
$G\,(t)$: Constant rate pressure drop function, psi
h : Formation thickness, ft
k : Formation permeability, md
k_k: Curvature constraints (Eq. (9))
K: Constant vector in curvature term
m: Number of pressure points (Eq. (6))
N_p: Number of pressure measurements (Eqs. (9) and (10))
N_q: Number of rate measurements (Eqs. (9) and (10))
N: Number of time nodes (curvature term in Eq. (9))

p_i: Measured pressure, psi (Eq. (9))
p_{mi}: Measured pressures, psi (NOF Eq. (10))
p_{Mi}: Estimated (calculated) pressures, psi (NOF Eq. (10))
p_0: Initial pressure in pressure match term, psi (Eqs. (5),(8), and (9))
$p_u(t_1)$: Pressure drop at the first time node, psi (Levitan)
p: Measured pressure, psi (Eqs. (5), and (8))
q_j: Measured flow rates, STB/D (Eq. (9))
q_{mj}: Measured rates, STB/D (NOF Eq. (10))
q_{Mj}: Estimated rates, STB/D (NOF Eq. (10))
q^u: Estimated flow rates, STB/D (Eq. (9))
q: Measured flow rate, STB/D
r_e: External radius, ft
r_w: Well radius, ft
t : Time, hr
w_{pi}: Weights of pressure error measure (Pimonov Eq. (9), NOF Eq. (10))
w_{qj} : Weights of rate data error measure (Pimonov Eq. (9), NOF Eq. (10))
Y_m: Vector with each component equal to 1 (von Schroeter Eq. (5), Levitan Eq. (7))
$\tilde{y}$: Flow rate at the time of each pressure measurement (Levitan Eq. (7))
y: Estimated flow rate, STB/D
z: well test pressure derivative on logarithmic scale (defined by Eq. (3).a)
Δp: Pressure drop data, psi
$\Delta p_{\text{model}}(t)$: Model estimated pressure drop, psi (Eq. (4) for von Schroeter model and Eq. (7) for Levitan model)
ζ_q: Error bound for rates, STB/D (Levitan Eq. (8))
ζ_p: Error bound for pressures, psi (Levitan Eq. (8))
ζ_c: Error bound for curvature (Levitan Eq. (8))
υ : Flow rate weight parameter (von Schroeter Eq. (5))
λ: Smoothing parameter (von Schroeter Eq. (5), and NOF Eq. (10))
σ: Selected time nodes (defined by Eq. (3).b)
σ_1: First time node (integral limit in Levitan model Eq. (7))
σ_p: Error bound for pressures (Pimonov et al Eq. (9))
σ_q: Error bound for rates (Pimonov et al. Eq. (9))
σ_c: Error bound for curvature (Pimonov et al. Eq. (9))

Abbreviations

DST: Drill Stem Test
NOF: New Objective Function

CRediT authorship contribution statement

Mina S. Khalaf: Conceptualization, Methodology, Software, Data curation, Investigation, Validation, Visualization, Writing- Original draft preparation, Writing- Reviewing and Editing.

Declaration of Competing Interest

The author declares that he has no known competing financial interests or personal relationships that could have appeared to influence the work reported in this paper.

Appendix A. von Schroeter Algorithm

This section provides details on the von Schroeter algorithm. The algorithm is a time domain method characterized by three novel ideas: (1) the error measure accounts for uncertainties not only in pressure, but also in rate data. The resulting formulation is known as a Total Least Squares (TLS) problem, (2) the algorithm uses implicit constraints on the parameters by encoding the response function in a way such that sign constraints are not necessary. This makes the problem nonlinear, and (3) the algorithm uses smoothness constraints based on a measure of the total curvature of the pressure derivative. Duhamel's principle (convolution equation) describes the pressure drop ΔP at time t as following:

$$\Delta p(t) = p_o - p(t) = \int_0^T q'(\tau)\, G(t-\tau)\mathrm{d}\tau = \int_0^T q(\tau)\, g(t-\tau)\mathrm{d}\tau \tag{A.1}$$

Where $g(t) = \mathrm{d}G/\mathrm{d}t$. p_0 is initial pressure, psi. $q(t)$ is flow rate function, BPD. $G(t)$ is rate normalized pressure drop function in psi. T is the test duration in hour. The implicit constraints is to parameterize the solution space such that the constraints ($g(t) > 0$) are automatically satisfied by using:

$$Z(\sigma) = \ln(t\, g(t)), \sigma = \ln(t) \tag{A.2}$$

Substituting Eq. (A.2) in Eq. (A.1):

$$\Delta p = \int_{-\infty}^{\ln(t)} \mathrm{e}^{Z(\sigma)}\, q(t - \mathrm{e}^{\sigma})\mathrm{d}\sigma \tag{A.3}$$

Time nodes (σ_k) are chosen such that:

$$-\infty = \sigma_0 < \sigma_1 < \cdots\cdots < \sigma_n = \ln(T) \tag{A.4}$$

The interpolation scheme of Z is linear (Fig. 2 left):

$$Z = \alpha_k + \beta_k \sigma,\ \sigma_{k-1} < \sigma < \sigma_k \tag{A.5}$$

The interpolation scheme of flow rate is a stepwise function (Fig. 2 right):

$$y(t) = \sum_j y_j\, \theta_j(t) \tag{A.6}$$

If y_j refers to a constant flow rate in some interval I_j, then

$$\theta_j(t) = \begin{cases} 1 & : t \in I_j \\ 0 & : t \notin I_j \end{cases} \tag{A.7}$$

By substituting Eq. (A.5) and (A.6) in Eq. (A.3), the following expression for the pressure signal is obtained:

$$p(t) = p_0 - \sum_{j=1}^{N} y_j\, G_j(Z, t) \tag{A.8}$$

$$G_j(z,t) = \sum_{k=1}^{n} \int_{\sigma_{k-1}}^{\sigma_k} \theta_j(t - \mathrm{e}^{\sigma})\, \mathrm{e}^{\alpha_k + \sigma\, \beta_k}\, \mathrm{d}\sigma \tag{A.9}$$

Eq. (A.8), in vector notation, can be written as following:

$$\Delta p = p_0 Y_m - p = C(Z)\, y \tag{A.10}$$

Eq. (A.10) is linear in the flow rates y_j and the initial pressure p_0, but nonlinear in the response parameters Z_k. The error measure (objective function) including the errors in the well test measurements and the smoothing term is:

$$E = \|p_0 Y_m - p - C(Z)\, y\|^2 + \nu \|y - q\|^2 + \lambda \|DZ - K\|^2 \tag{A.11}$$

Where the term $\|P_0 Y_m - P - C(Z) \quad y\|^2$ accounts for the error in the pressure data, the term $\|y - q\|^2$ accounts for error in flow rate measurements, and the term $\|DZ - K\|^2$ is a measure of the smoothness of Z. p_0 is initial pressure. Y_m is vector with components of 1. y is vector of true rates. q is vector of measured rates. D is constant matrix of size $(n-1) \times n$. K is constant vector $(1,0,\ldots\ldots 0) \epsilon \mathbb{R}^{n-1}$. ν and λ are adjustable weights.

The constant matrix D can be written as:

$$D_{1j} = \begin{cases} -(\sigma_2 - \sigma_1)^{-1}, & j = 1 \\ (\sigma_2 - \sigma_1)^{-1}, & j = 2 \\ 0, & j = 3, \ldots, n \end{cases} \tag{A.12}$$

$$D_{ij} = \begin{cases} (\sigma_i - \sigma_{i-1})^{-1}, & j = i - 1 \\ -\dfrac{\sigma_{i+1} - \sigma_{i-1}}{(\sigma_{i+1} - \sigma_i)(\sigma_i - \sigma_{i-1})}, & j = i \\ (\sigma_{i+1} - \sigma_i)^{-1}, & j = i + 1 \\ 0, & \text{otherwise} \end{cases} \tag{A.13}$$

In case of uniform spacing with step size h, rows 2 to n-1 of D reduce to the well-known discrete approximation of a second derivative operator with $\frac{-2}{h}$ in the diagonal and h^{-1} in the sub-diagonal and super-diagonal.

Eq. (A.11) can be written in the form:

$$E(y, Z) = F(Z)x - \nu(Z) \tag{A.14}$$

$$F(Z) = \begin{bmatrix} Y_m & -C(Z) \\ 0 & \sqrt{\nu} \\ 0 & 0 \end{bmatrix} \tag{A.15}$$

$$\nu(Z) = \begin{bmatrix} p \\ \sqrt{\nu}\, q \\ \sqrt{\lambda}\, (DZ - K) \end{bmatrix} \tag{A.16}$$

$$x = [p_0, y]^T \tag{A.17}$$

The expression for the matrix C is:

$$C_{ij}(Z) = \sum_{k=1}^{n} \mathrm{e}^{\alpha_k}\, C_{ijk}(Z) \tag{A.18}$$

$$C_{ijk}(Z) = \begin{cases} 0 & : I_{ijk} = \varphi \\ \beta_k^{-1}\, \mathrm{e}^{b\beta_k} & : a = -\infty \\ 2\rho & : a \neq -\infty,\ \beta_k = 0 \\ 2\beta_k^{-1}\, \mathrm{e}^{\mu\beta_k} \sinh(\rho\beta_k) & : a \neq -\infty,\ \beta_k \neq 0 \end{cases} \tag{A.19}$$

$I_{ijk} = \{\sigma \in (\sigma_{k-1}, \sigma_k) : \theta_j(t_i - \mathrm{e}^{\sigma}) = 1\}$, $k = 1,\ldots,n$. I_{ijk} is either empty, a semi-infinite interval $(-\infty, b]$, or a finite interval $[a, b] = [\mu - \rho, \mu + \rho]$ with mid point μ and radius ρ.

This deconvolution problem is equivalent to a separable nonlinear total least squares problem. One of the standard algorithms for this class of problems is the variable projection algorithm. The variable projection algorithm requires Jacobian of the residue $E(y, Z)$ with respect to the nonlinear parameters (Z). Jacobian components are:

$$\frac{\partial C_{ij}}{\partial Z_k} = \begin{cases} e^{\alpha_1} C_{ij1}(Z) + e^{\alpha_2} \dfrac{D_{ij2}(Z) - \sigma_2\, C_{ij2}(Z)}{\sigma_1 - \sigma_2}, & \text{for } k = 1 \\ e^{\alpha_k} \dfrac{D_{ijk}(Z) - \sigma_{k-1}\, C_{ijk}(Z)}{\sigma_k - \sigma_{k-1}} + e^{\alpha_{k+1}} \dfrac{D_{ij,k+1}(Z) - \sigma_{k+1}\, C_{ij,k+1}(Z)}{\sigma_k - \sigma_{k+1}}, & \text{for } k = 2, \ldots, n-1 \\ e^{\alpha_n} \dfrac{D_{ijn}(Z) - \sigma_{n-1}\, C_{ijn}(Z)}{\sigma_n - \sigma_{n-1}}, & \text{for } k = n \end{cases} \tag{A.20}$$

$$D_{ijk} = \begin{cases} 0 & : I_{ijk} = \varphi \\ (b\beta_k^{-1} - \beta_k^{-2}) e^{b\beta_k} & : a = -\infty \\ 2\mu\rho & : a \neq -\infty,\ \beta_k = 0 \\ 2\beta_k^{-1} \quad e^{\mu\beta_k}\left((\mu - \beta_k^{-1}) \sinh(\rho\beta_k) + \rho \cosh(\rho\beta_k)\right) & : a \neq -\infty,\ \beta_k \neq 0 \end{cases} \tag{A.21}$$

The first node σ_1 should be early enough to ensure that the region $\sigma < \sigma_1$ corresponds to wellbore storage. The starting point for the iteration (y_0, Z_0) is required. For y_0, an estimate for the initial pressure p_0 is obtained as the maximum of the pressure data followed by the measured rates. For Z_0, unit slope line is used before σ_1 and constant value afterwards.

$$Z_0 = \begin{cases} \ln(c_0) + \sigma & : \sigma \leq \sigma_1 \\ \ln(c_1) & : \sigma \geq \sigma_1 \end{cases} \tag{A.22}$$

$$\ln(c_0) = \ln(c_1) - \sigma_1 \tag{A.23}$$

The value c_1 is determined such that the best pressure fit is obtained. Evaluating Eq. (A.3) with the model of Eq. (A.22) leads to:

$$\Delta p(t) = c_0 \Delta p_1(t) + c_1 \sum\nolimits_j q_j \mu_j(t) \tag{A.24}$$

$$\mu_j(t) = \int_{\sigma_1}^{\ln(T)} \theta_j(t - e^{\sigma}) d\sigma \tag{A.25}$$

By choosing the first node early enough, the contribution ΔP_1 from the early part can be made arbitrary small. Therefore, remaining part only is evaluated. The error in vector notation is given by:

$$\varepsilon = c_1 M q - \Delta p \tag{A.26}$$

$$c_1 = \frac{\Delta P^T M q}{\|M q\|^2} \tag{A.27}$$

$$M = \begin{pmatrix} \mu_1(t_1) & \mu_2(t_1) & \cdots & \mu_N(t_1) \\ \mu_1(t_2) & \mu_2(t_2) & \cdots & \mu_N(t_2) \\ \vdots & \vdots & \vdots & \vdots \\ \mu_1(t_m) & \mu_2(t_m) & \cdots & \mu_N(t_m) \end{pmatrix} \tag{A.28}$$

The algorithm is stable in the sense that the results do not depend on the starting point. The choice has the merit of reducing the number of iterations required for convergence.

The criteria for the selection of the weights μ and λ are simply $\nu = \frac{N}{m} \frac{||\Delta p||^2}{||q||^2}$, and $\mu = \frac{\|\Delta p\|^2}{m}$ where N is the number of flow periods and m is the number of pressure data points.

Appendix B. Levitan Algorithm

Levitan introduced an enhancement to von Schroeter algorithm to be used reliably with real test data. Levitan pulled the first time-node out of the integral such that the problem is optimized with no restrictions before that first node. This allows the deconvolution algorithm to handle wellbore-storage-free transient data by overcoming the unit slope straight line assumption before the first time node in von Schroeter algorithm. If the first time-node is chosen to be small enough, the convolution integral can be written as:

$$p(t) = p_0 - q(t_i) p_u(t_1) - \int_{\sigma_1}^{\ln(t_i)} q(t_i - e^{\sigma}) e^{z(\sigma)} d\sigma \tag{B.1}$$

where $p_u(t_1)$ is the pressure drop at the first time-node.

Following a linear interpolation scheme for the pressure derivative and a stepwise scheme for the flow rate, as discussed in Appendix A for von Schroter algorithm, the final form of Levitan's objective function can be written as:

$$\Phi(x) = \frac{1}{2}\sum_{i=1}^{M}\left[\frac{\omega_i - \Omega_i(x)}{\varsigma_i}\right]^2 \tag{B.2}$$

where $\omega = \{\omega_p, \quad \omega_q, \quad \omega_c\}$ is vector of constraints. $\Omega_i(x)$ is model prediction which depends on model parameters. $\varsigma = \{\varsigma_1, \varsigma_2, \quad \ldots, \varsigma_M\}$ is vector of error bound estimates for the data points.

This function may have many local minima and the minimization process may converge to any one of them. Selection of the initial vector of model parameters is critically important for successful minimization. The parameter $p_u(t_1)$ is initialized to unity. The remaining response function parameters $z(\sigma)$ are initialized to a constant value c_1(the same as von Schroeter initialization). The rate parameters, $q(t)$, are initialized to the corresponding values of rate constraints. The initial pressure (p_0) is set to the maximum pressure in the measured data.

References

[1] Y. Osman, A. Retnanto, M. Samir, et al., Enhancing pressure transient analysis through the application of deconvolution methods, case study, SPE Middle East Oil & Gas Show and Conference. 6-9 March , 2017. Manama, Kingdom of Bahrain (2017) SPE-184022-MS, https://doi.org/10.2118/184022-ms.

[2] M.S. Khalaf, N. Soliman, A.H. El-Banbi, Wellbore storage removal in pressure transient analysis for gas wells, J. Pet. Sci. Eng. 208 (2022) 109712.

[3] A.F. van Everdingen, W. Hurst, The application of the Laplace transformation to flow problems in reservoirs, J. Pet. Technol. 1 (12) (1949) 305–324.

[4] T.S. Hutchinson, V.J. Sikora, A generalized water-drive analysis, Trans. AIME 216 (1) (1959) 169–178.

[5] T. Von Schroeter, F. Hollaender, A.C. Gringarten, Deconvolution of well-test data as a nonlinear Total Least-Squares problem, SPE J. 9 (4) (2004) 375–390, https://doi.org/10.2118/77688-PA.

[6] M.M. Levitan, Practical application of pressure / rate deconvolution to analysis of real well tests, SPE Reserv. Eval. Eng. 8 (2) (2005) 113–121.

[7] D. Ilk, P.P. Valkó, T.A. Blasingame, Deconvolution of variable-rate reservoir-performance data using B-splines, SPE Reserv. Eval. Eng. 9 (5) (2006) 582–595.

[8] M. Onur, F.J. Kuchuk, A new deconvolution technique based on pressure-derivative data for pressure-transient-test interpretation, SPE J. 17 (1) (2012) 307–320, https://doi.org/10.2118/134315-PA.

[9] M. Nomura, R.N. Horne, Data processing and interpretation of well test data as a nonparametric regression problem, SPE Western Regional Meeting. 24–26 March, 2009. San Jose, California, USA (2009) SPE 120511-MS, https://doi.org/10.2118/120511-ms.

[10] A. Chen, J.R. Jones, Use of pressure / rate deconvolution to estimate connected reservoir-drainage volume in naturally fractured unconventional-gas reservoirs from Canadian Rockies foothills, SPE Reserv. Eval. Eng. 15 (3) (2012) 290–299.

[11] J.A. Cumming, D.A. Wooff, T. Whittle, et al., Assessing the non-uniqueness of the well test interpretation model using deconvolution, EAGE Annual Conference & Exhibition Incorporating SPE Europec. 10–13 June, 2013. London, United Kingdom (2013) SPE 164870-MS, https://doi.org/10.2118/164870-ms.

[12] A. Gringarten, Practical use of well test deconvolution, SPE Annual Technical Conference and Exhibition. 20–22 September, 2010. Florence, Italy (2010) SPE 134534-MS, https://doi.org/10.2118/134534-MS.

[13] A.C. Gringarten, From straight lines to deconvolution: The evolution of the state of the art in well test analysis, SPE Reserv. Eval. Eng. 11 (1) (2008) 41–62.

[14] M.M. Levitan, M.R. Wilson, Deconvolution of pressure and rate data from gas reservoirs with significant pressure depletion, SPE J. 17 (3) (2012) 727–741. https://doi.org/10.2118/134261-PA.

[15] M. Onur, M. Cinar, D. Ilk, et al., An investigation of recent deconvolution methods for well-test data analysis, SPE J. 13 (2) (2008) 226–247. https://doi.org/10.2118/102575-PA.

[16] E.A. Pimonov, M. Onur, F.J. Kuchuk, A new robust algorithm for solution of pressure/rate deconvolution problem, J. Inverse Ill. Posed Probl. 17 (6) (2009) 611–627.

[17] J.H. Wu, D. Georgi, E. Ozkan. Deconvolution of wireline formation test data, SPE Annual Technical Conference and Exhibition. 4–7 October, 2009. New Orleans, Louisiana, USA (2009) SPE 124220-MS, https://doi.org/10.2118/124220-MS.

[18] Y. Cheng, W.J. Lee, D.A. Mcvay, Application of fast Fourier transforms to deconvolution of multirate well test data, SPE Annual Technical Conference and Exhibition. 9-12 October, 2005. Dallas, Texas (2005) SPE 96032-MS, https://doi.org/10.2118/96032-MS.

[19] M.S. Khalaf, A.H. El-Banbi, M.H. Sayyouh, New technique revives direct deconvolution methods for Wellbore storage removal in pressure transient analysis, Egypt J. Pet. 30 (2) (2021) 37–43.

[20] M.S. Khalaf, A.H. El-Banbi, A. El-Maraghi, et al., Two-step deconvolution approach for wellbore storage removal, J. Pet. Sci. Eng. 195 (2020) 107827.

[21] R. Geravand, J. Foroozesh, A. Nakhaee, et al., Well-test deconvolution analysis of gas condensate layered reservoirs, Offshore Technology Conference Asia. 2–6 November, 2020. Kuala Lumpur, Malaysia (2020) OTC-30291-MS, https://doi.org/10.4043/30291-ms.

[22] J.A. Cumming, D.A. Wooff, T. Whittle, et al., Multiwell deconvolution, SPE Reserv. Eval. Eng. 17 (4) (2014) 457–465.

[23] Y. Tung, C. Virues, J. Cumming, et al., Multiwell deconvolution for shale gas, SPE Europec Featured at 78th EAGE Conference and Exhibition. 30 May–2 June, 2016. Vienna, Austria (2016) SPE-180158-MS, https://doi.org/10.2118/180158-MS.

[24] W.C. Liu, C.C. Qiao, P. Wang, et al., Study of inter-well interference in shale gas reservoirs by a robust production data analysis method based on deconvolution, Pet. Sci. 21 (4) (2024) 2502–2519.

[25] R.A. Beier, Deconvolution and convolution methods for thermal response tests on borehole heat exchangers, Geothermics 86 (2020) 101786.

[26] A. AlNaqbi, S. AlMuhairi. An innovative approach towards improving pressure transient analysis for a tight oil formation: A case study, ADIPEC. 2–5 October, 2023. Abu Dhabi, UAE (2023) SPE-216466-MS, https://doi.org/10.2118/216466-MS.

[27] R.B. Piccinini, L.K. Kubota, M.R. Galvão, et al., Application of an ensemble-based method for pressure-rate deconvolution, SPE J. 30 (9) (2025) 5612–5629. https://doi.org/10.2118/220707-PA.

[28] T. Botsas, J.A. Cumming, I.H. Jermyn, A Bayesian multi-region radial composite reservoir model for deconvolution in well test analysis, J. R. Stat. Soc. Ser. C. Appl. Stat. 71 (4) (2022) 951–968.

[29] K.A.M.H. Abdalla, H. Khattab, M. Tantawy, et al., Enhancing pressure transient analysis in reservoir characterization through deep learning neural networks, Discov. Appl. Sci. 6 (9) (2024) 473.

[30] S.T. Nukala, A. Kumar, S. Rajput, et al., Enhancing pressure transient analysis with automatic model identification: A machine learning approach, SPE Western Regional Meeting. 16-18 April, 2024. Palo Alto, California, USA (2024) SPE 218836-MS, https://doi.org/10.2118/218836-MS.

[31] D.F. Rossi, M.C.B. da Costa, K.S. Komati, Evaluation of automated pressure transient detection methods for efficient oil well management, Geoenergy Sci. Eng. 257 (2026) 214202.

[32] M.R.A. Juneghani, S. Moradi, M.R. Zavelaneh, et al., A comprehensive review of analytical solutions and advances in pressure transient analysis of conventional reservoirs, J. Pet. Explor Prod. Technol. 15 (5) (2025) 101.

[33] E. Pimonov, C. Ayan, M. Onur, et al., New pressure / rate-deconvolution algorithm to analyze wireline- formation-tester and well-test data, SPE Reserv. Eval. Eng. 13 (4) (2010) 603.

[34] J.P. Spivey, W.J. Lee, Applied well test interpretation. Richardson: Society of Petroleum Engineers, Texas, USA, 2013, https://doi.org/10.2118/9781613993071.

[35] J. Cahill, K. Dinsdale, Increasing Accuracy Multiph. Flow. Meas. (2025). ⟨https://www.emersonautomationexperts.com/2025/industry/oil-gas/increasing-accuracy-multiphase-flow-measurement/⟩ (accessed January 1, 2025).

[36] SLB. SLB's permanent monitoring systems 2025. ⟨https://www.slb.com/products-and-services/innovating-in-oil-and-gas/completions/well-completions/permanent-monitoring/permanent-downhole-gauges?currentPage=2&itemId=af6c75f1-647b-441c-b199-594f7c5e5ce0⟩ (accessed January 1, 2025).

[37] F.J. Kuchuk, M. Onur, F. Hollaender. Pressure transient formation and well testing: Convolution, deconvolution and nonlinear estimation, Developments in Petroleum Science, 57, first ed., Elsevier B.V, 2010 https://doi.org/10.1016/S0376-7361(10)05710-9.

[38] Å. Björck. Numerical methods for least squares problems. Society for Industrial and Applied Mathematics 3600, University City Science Center, Philadelphia, PA, 1996 19104-2688, https://doi.org/10.1137/1.9781611971484.

[39] D.P. O'Leary, B.W. Rust, Variable projection for nonlinear least squares problems, Comput. Optim. Appl. 54 (3) (2013) 579–593.

[40] E. Pimonov, C. Ayan, M. Onur, et al., A New pressure/rate deconvolution algorithm to analyze wireline formation tester and well-test data, SPE Annual Technical

Conference and Exhibition. 4–7 October, 2009. New Orleans, Louisiana, USA (2009) SPE 123982, https://doi.org/10.2118/123982-ms.
[41] J.E. Dennis, R.B. Schnabel, Numerical methods for unconstrained optimization and nonlinear equations. Engle Wood Cliffs, Prentice-Hall Inc, New Jersy, 1983.
[42] O.R. Green, Y.L. Bao, J.R. Lawall, et al., Accurate, precise pressure sensing with tethered optomechanics, ArXiv Cornell Univ (2024) 20899. https://arxiv.org/abs/2409.00256.
[43] R.B. Piccinini, L.K. Kubota, M.R. Galvão, et al., Application of an ensemble based method for pressure-rate deconvolution, SPE Annual Technical Conference and Exhibition. 23–25 September, 2024. New Orleans, Louisiana, USA (2024) SPE-220707-MS, https://doi.org/10.2118/220707-MS.
[44] D. Bourdet, J.A. Ayoub, Y.M. Plrard, Use of pressure derivative in well-test interpretation, SPE Form. Eval. 4 (2) (1989) 293–302.

Dr. Mina S. Khalaf is a Research Scientist supporting the U.S. Department of Energy's National Energy Technology Laboratory. He holds a Ph.D. in Petroleum Engineering from the University of Houston and has over ten years of combined research and industry experience in reservoir engineering, geothermal energy, computational geomechanics, and well test analysis. His work includes advancements in carbon storage, hydraulic and plasma fracturing, machine learning for subsurface applications, and pressure transient analysis, with multiple peer-reviewed publications in petroleum and energy engineering.